A&A 530, A80 (2011)
DOI: 10.1051/0004-6361/201116681

Astronomy & Astrophysics

Observing pulsars and fast transients with LOFAR

B. W. Stappers[1], J. W. T. Hessels[2,3], A. Alexov[3], K. Anderson[3], T. Coenen[3], T. Hassall[1], A. Karastergiou[4], V. I. Kondratiev[2], M. Kramer[5,1], J. van Leeuwen[2,3], J. D. Mol[2], A. Noutsos[5], J. W. Romein[2], P. Weltevrede[1], R. Fender[6], R. A. M. J. Wijers[3], L. Bähren[3], M. E. Bell[6], J. Broderick[6], E. J. Daw[8], V. S. Dhillon[8], J. Eislöffel[19], H. Falcke[12,2], J. Griessmeier[2,22], C. Law[24,3], S. Markoff[3], J. C. A. Miller-Jones[13,3], B. Scheers[3], H. Spreeuw[3], J. Swinbank[3], S. ter Veen[12], M. W. Wise[2,3], O. Wucknitz[17], P. Zarka[16], J. Anderson[5], A. Asgekar[2], I. M. Avruch[2,10], R. Beck[5], P. Bennema[2], M. J. Bentum[2], P. Best[15], J. Bregman[2], M. Brentjens[2], R. H. van de Brink[2], P. C. Broekema[2], W. N. Brouw[10], M. Brüggen[21], A. G. de Bruyn[2,10], H. R. Butcher[2,26], B. Ciardi[7], J. Conway[11], R.-J. Dettmar[20], A. van Duin[2], J. van Enst[2], M. Garrett[2,9], M. Gerbers[2], T. Grit[2], A. Gunst[2], M. P. van Haarlem[2], J. P. Hamaker[2], G. Heald[2], M. Hoeft[19], H. Holties[2], A. Horneffer[5,12], L. V. E. Koopmans[10], G. Kuper[2], M. Loose[2], P. Maat[2], D. McKay-Bukowski[14], J. P. McKean[2], G. Miley[9], R. Morganti[2,10], R. Nijboer[2], J. E. Noordam[2], M. Norden[2], H. Olofsson[11], M. Pandey-Pommier[9,25], A. Polatidis[2], W. Reich[5], H. Röttgering[9], A. Schoenmakers[2], J. Sluman[2], O. Smirnov[2], M. Steinmetz[18], C. G. M. Sterks[23], M. Tagger[22], Y. Tang[2], R. Vermeulen[2], N. Vermaas[2], C. Vogt[2], M. de Vos[2], S. J. Wijnholds[2], S. Yatawatta[10], and A. Zensus[5]

(Affiliations can be found after the references)

Received 9 February 2011 / Accepted 22 March 2011

ABSTRACT

Low frequency radio waves, while challenging to observe, are a rich source of information about pulsars. The LOw Frequency ARray (LOFAR) is a new radio interferometer operating in the lowest 4 octaves of the ionospheric "radio window": 10–240 MHz, that will greatly facilitate observing pulsars at low radio frequencies. Through the huge collecting area, long baselines, and flexible digital hardware, it is expected that LOFAR will revolutionize radio astronomy at the lowest frequencies visible from Earth. LOFAR is a next-generation radio telescope and a pathfinder to the Square Kilometre Array (SKA), in that it incorporates advanced multi-beaming techniques between thousands of individual elements. We discuss the motivation for low-frequency pulsar observations in general and the potential of LOFAR in addressing these science goals. We present LOFAR as it is designed to perform high-time-resolution observations of pulsars and other fast transients, and outline the various relevant observing modes and data reduction pipelines that are already or will soon be implemented to facilitate these observations. A number of results obtained from commissioning observations are presented to demonstrate the exciting potential of the telescope. This paper outlines the case for low frequency pulsar observations and is also intended to serve as a reference for upcoming pulsar/fast transient science papers with LOFAR.

Key words. telescopes – pulsars: general – instrumentation: interferometers – methods: observational – stars: neutron – ISM: general

1. Introduction

Pulsars are rapidly rotating, highly magnetised neutron stars that were first identified via pulsed radio emission at the very low radio observing frequency of 81 MHz (Hewish et al. 1968). They have subsequently been shown to emit pulsations across the electromagnetic spectrum, at frequencies ranging from 17 MHz to above 87 GHz (e.g. Bruk & Ustimenko 1976, 1977; Morris et al. 1997) in the radio and at optical, X-ray and γ-ray wavelengths (see Thompson 2000, and references therein), although the vast majority are seen to emit only at radio wavelengths. These pulsations provide invaluable insights into the nature of neutron star physics, and most neutron stars would be otherwise undetectable with current telescopes. Though radio pulsars form over 85% of the known neutron star population, they are generally very weak radio sources with pulsed flux densities ranging from 0.0001 to 5 Jy with a median of 0.01 Jy at a frequency of 400 MHz. The pulsed flux density at radio wavelengths exhibits a steep spectrum ($S \propto \nu^{\alpha}$; $-4 < \alpha < 0$; $\alpha_{\rm mean} = -1.8$, Maron et al. 2000) that often peaks and turns over at frequencies between 100 and 200 MHz (Kuzmin et al. 1978; Slee et al. 1986; Malofeev et al. 1994).

After their discovery, a lot of the early work on pulsars (e.g. Cole 1969; Staelin & Reifenstein 1968; Rankin et al. 1970) continued at low radio frequencies (defined here as <300 MHz). However, despite the fact that most pulsars are intrinsically brightest in this frequency range, since then the vast majority of pulsars have been discovered and studied at frequencies in the range 300–2000 MHz; much of our knowledge of the properties of the radio emission mechanism stems from studies at these frequencies and above. There are three main reasons for this (see Sect. 3): the deleterious effects of the interstellar medium (ISM) on pulsed signals; the effective background sky temperature of the Galactic synchrotron emission; and ionospheric effects. All three of these effects have steep power law dependencies on frequency and therefore become worse towards lower frequencies. Combined with the generally steep spectra of pulsars, these effects conspire to make observing frequencies of ~300−2000 MHz the range of choice for most pulsar studies and searches.

However, despite these challenges, there are many reasons why it is important and interesting to observe pulsars in a significantly lower frequency regime than now commonly used; these are discussed in detail in Sect. 4. In recent years some excellent

Fig. 1. Three successive zoom-outs showing the stations in the LOFAR core. The different scales of the hierarchically organised HBA elements are highlighted and their respective beam sizes are shown. The large circular area marks the edge of the Superterp, which contains the inner-most 6 stations (i.e. 12 HBA sub-stations: where there are 2 sub-stations, each of 24 tiles, in each HBA core station); other core stations can be seen highlighted beyond the Superterp in the third panel. *Left*: a single HBA tile and associated beam. *Middle*: a single HBA sub-station with three simultaneous station beams. *Right*: the 6 stations of the Superterp plus 3 core stations in the background are highlighted. Four independent beams formed from the coherent combination of all 24 core HBA stations, most of which are outside this photo, are shown. For the LBA stations, a similar scheme applies except that each LBA dipole can effectively see the whole sky. Fields of the relatively sparsely distributed LBA antennas are visible in between the highlighted HBA stations in all three panels.

studies have continued at frequencies between 20−110 MHz mainly using the Pushchino, Gauribidanur and UTR-2 telescopes (e.g. Malov & Malofeev 2010; Malofeev et al. 2000; Asgekar & Deshpande 2005; Popov et al. 2006b; Ulyanov et al. 2006). These studies have begun to map, e.g., the low-frequency spectra, pulse morphologies, and pulse energy distributions of pulsars, but have in some cases been limited by the available bandwidths and/or polarisation and tracking capabilities of these telescopes (see Sect. 2).

The LOw Frequency ARray (LOFAR) was designed and constructed by ASTRON, the Netherlands Institute for Radio Astronomy, and has facilities in several countries, that are owned by various parties (each with their own funding sources), and that are collectively operated by the International LOFAR Telescope (ILT) foundation under a joint scientific policy. LOFAR provides a great leap forward in low-frequency radio observations by providing large fractional bandwidths and sophisticated multi-beaming capabilities. In this paper we present the LOFAR telescope as it will be used for pulsar and other high-time-resolution beamformed observations; this will serve as a reference for future science papers that use these LOFAR modes. We also describe the varied pulsar and fast transient science LOFAR will enable and present commissioning results showing how that potential is already being realised. LOFAR is well suited for the study of known sources, and its huge field of view (FoV) makes it a powerful survey telescope for finding new pulsars and other "fast-transients". In Sect. 2 we present the basic design parameters of the LOFAR telescope. The challenges associated with observing at low radio frequencies and how they can be mitigated with LOFAR will be discussed in Sect. 3. A detailed description of the science that will be possible with LOFAR is presented in Sect. 4. The flexible nature of LOFAR means that there are many possible observing modes; these are introduced in Sect. 5. In Sect. 6 we discuss the different pulsar pipelines that are being implemented. Commissioning results, which demonstrate that LOFAR is *already* performing pulsar and fast transients observations of high quality, are presented in Sect. 7. We summarise the potential of LOFAR for future pulsar observations in Sect. 8.

Table 1. Arrangement of elements in LOFAR stations.

Station type	LBA (No.)	HBA tiles (No.)	Baseline (km)
Core	2×48	2×24	0.1–1
Remote	2×48	48	1–10 s
International	96	96	~100 s

Notes. Arrangement of elements in the three types of LOFAR stations, along with their typical distance from the center of the array (baseline). In the Core and Remote stations there are 96 LBA dipoles but only 48 can be beamformed at any one time. For these stations, one can select either the inner circle or the outer ring of 48 LBA dipoles depending on the science requirements. The HBA sub-stations can be correlated, or used in beamforming, independently.

2. LOFAR

Instrumentation in radio astronomy is undergoing a revolution that will exploit massive computing, clever antenna design, and digital signal processing to greatly increase the instantaneous FoV and bandwidth of observations. This work is part of the international effort to create the "Square Kilometre Array" (Carilli & Rawlings 2004), a radio telescope orders of magnitude better than its predecessors.

One of the first "next generation" radio telescopes to implement these techniques is LOFAR, which operates in the frequency range 10–240 MHz. The large collecting area of LOFAR is comprised of many thousands of dipole antennas, hierarchically arranged in stations which come in three different configurations (Table 1). These stations are distributed in a sparse array with a denser core region near Exloo, the Netherlands, extending out to remote stations in the Netherlands and then on further to stations in France, Germany, Sweden and the United Kingdom. There are a total of 40 stations in the Netherlands and

Table 2. Comparison of some telescopes that have operated at frequencies below 200 MHz.

Telescope	Area (m^2)	T_{rec} (K)	T_{sky} (K)	Frequencies (MHz)	Bandwidth (MHz)	*N*bits	Beams	Transit
Arecibo	30 000		5700–5000	47–50			1	Restricted
Cambridge 3.6 ha	36 000		1400	81.5	1	1	16	Yes
DKR-1000	5000–8000		18 000–500	30–120	1–2			Yes
Gauribidanur	12 000	500	30 000–12 000	25–35	2	2	1	Yes
GMRT	48 000	295	276	151	16/32	8/4	2	No
LOFAR (LBA)	75 200	500	320 000–1000	10–90	48	16	<244	No
LOFAR (HBA)	57 000	140–180	630–80	110–240	48	16	<244	No
LWA	1 000 000		320 000–1100	10–88	19.2	8	4	No
MRT	41 000	500	276	~150	2	2	1	Yes
MWA	8000	150	1400–45	80–300	32	5	16(32)	No
Nançay Decametric Array	4000		320 000–800	10–100	32	14	1	No
LPA/BSA – Pushchino	20 000	110	900	109–113	2.5	12	16(32)	Yes
UTR-2	150 000		550 000–9000	8–40	24	16	5(8)	No
VLA	13 000		1800	74	1.56	2	1	No
WSRT	7000	400	650–175	110–180	8×2.5	8	1	No

Notes. Telescopes that are observing in (parts of) the same frequency range or have done so in the past are considered. The bandwidths presented are those that are used for pulsar observations and do not take into consideration what fraction may not be useful due to radio frequency interference. In the case of LOFAR pulsar observations, only a small fraction of the bandwidth requires masking (see Sect. 6). Note that the collecting area is the maximum and does not take into account efficiencies or hour angle dependent effects. The transit instruments such as the Mauritius Radio Telescope (MRT, Golap et al. 1998), Gauribidanur (Deshpande et al. 1989), and the Cambridge 3.6 ha telescope (Shrauner et al. 1998) have some tracking ability but are usually limited to observing times of a few minutes. The collecting area of Arecibo is based on an illumination equivalent to a 200 m dish. The collecting area for the UTR-2 (Abranin et al. 2001) is quoted for a frequency of 20 MHz and the 5-beam and 8-beam modes are discussed in Ryabov et al. (2010) and Abranin et al. (2001) respectively. The Murchison Widefield Array (MWA) can have 32 single polarisation beams and the area is quoted for a frequency of 200 MHz (Lonsdale et al. 2009). LOFAR can have up to a total of 244 station beams which equals the number of subbands. The Long Wavelength Array (LWA) (Ellingson et al. 2009) collecting area is quoted for a frequency of 20 MHz and decreases as λ^2. We note that the LWA and MWA collecting areas are those projected for the final system and are not yet in place. For the LOFAR LBA entry, the effective area is based on using the outermost antenna configuration at a freqeuncy of 30 MHz, which maximizes collecting area. The HBA collecting area is quoted for a frequency of 150 MHz. The GMRT (Swarup et al. 1991), VLA (Cohen et al. 2007) and WSRT (Karuppusamy et al. 2011) are multiple dish interferometers. In some cases, not all parameters are available in the literature and so these entries were left blank. T_{sky} is an approximate value calculated on a cold piece of sky and is quoted for the full range of available frequencies at that telescope.

8 international stations, with the prospect of more to come. A schematic diagram of some of the LOFAR stations in the inner core of LOFAR – the "Superterp" as it is known – is shown in Fig. 1. As will be discussed in more detail later, pulsar observations can utilise all of these stations to achieve a variety of diverse science goals. Details of system architecture and signal processing can be found in de Vos et al. (2009) and a full description of LOFAR will soon be published (van Haarlem et al., in prep.) we limit the discussion only to the most important points related to pulsar observations.

LOFAR has two different types of antennas to cover the frequency range 10–240 MHz. The low band antennas, LBAs, cover the frequency range 10–90 MHz, although they are optimised for frequencies above 30 MHz. The lower limit of 10 MHz is defined by transmission of radio waves through the Earth's ionosphere. There are 48/96 active LBA dipoles in each Dutch/international station (Table 1). The high band antennas, HBAs, cover the frequency range 110–240 MHz, and consist of 16 folded dipoles grouped into tiles of 4×4 dipoles each, which are phased together using an analogue beamformer within the tile itself. There are 48/96 tiles in each Dutch/international station, with a separation into two sub-stations of 24 HBA tiles each in the case of core stations[1].

The received radio waves are sampled at either 160 or 200 MHz in one of three different Nyquist zones to access the frequency ranges 0–100, 100–200 and 160–240 MHz. There are filters in place to optionally remove frequencies below 30 MHz and the FM band approximately encompassing 90–110 MHz. The 80 or 100 MHz wide bands are filtered at the stations into 512 subbands of exactly 156.25/195.3125 kHz using a polyphase filter. Up to 244 of these subbands can be transported back to the Central Processor, CEP, giving a maximum instantaneous bandwidth of about 39/48 MHz[2]. There is no restriction on which 244 of the 512 subbands can be selected to be processed at CEP, therefore this bandwidth can be distributed throughout the entire available 80/100 MHz. Alternatively it is possible to portion out the bandwidth into multiple beams. Previously there was a limit of eight per station, however a recent new implementation of the beam server software has enabled each of the 244 subbands to be pointed in a different direction. These subbands can be further divided into narrower frequency channels in CEP as will be discussed below. The degree of flexibility afforded by these choices of frequency and beams allows a wide range of high-time-resolution pulsar-like observations with LOFAR; these different modes are described in detail in Sect. 5.

In Table 2 we compare the properties of LOFAR with those of other telescopes currently operating in (part of) the same frequency range. LOFAR is the *only* existing or planned telescope capable of covering the entire lowest 4 octaves of the radio window (10–240 MHz, above the Earth's ionospheric cut-off). In some modes this entire range can be observed simultaneously

[1] We note that when we refer to dipoles and tiles we are generally referring to both the *X* and *Y* polarisations together, that is dipole pairs, and we draw a distinction between the two polarisations only when necessary.

[2] This number may further increase if the number of bits used to describe each sample is reduced.

(see Sect. 5). LOFAR's total effective collecting area and instantaneous sensitivity places it at the forefront of existing low-frequency radio telescopes, especially in the range 100–240 MHz, but collecting area is only one aspect of LOFAR's capabilities. As will be described in more detail later, LOFAR offers many advantages over current telescopes through its multi-beaming capabilities, flexible backend, high spatial resolution, large instantaneous bandwidth, wide total available frequency range, ability to track, and ability to observe a large fraction of the sky (i.e. declinations greater than −30 degrees, see Sect. 5).

3. Challenges of observing at low frequencies

As previously mentioned, currently the majority of radio pulsar observations are done between 300–2000 MHz because this frequency range greatly reduces the severity of several low-frequency observational impediments. Here we describe these challenges in more detail and explain how LOFAR is capable of mitigating them.

3.1. Interstellar medium

Simply put, effects in the ISM between the observer and the pulsar degrade the effective time resolution of the data and, in severe cases, completely mask short time-scale variations like the typically milliseconds-wide pulses of pulsars. Free electrons in the ISM between the pulsar and the Earth cause the pulsed signal to be both dispersed and scattered. Dispersion results in the pulses at lower frequencies being delayed relative to those at higher frequencies. This effect is directly proportional to the number of free electrons along the line of sight, which is expressed as the dispersion measure (DM); the quadratic frequency dependence of the delay means the effect is particularly severe when observing with even 1% fractional bandwidths at frequencies below 200 MHz. For example, at a central frequency of 100 MHz and using a bandwidth of 2 MHz the pulses from a pulsar with a relatively low DM of 20 pc cm^{-3} will be smeared out by ∼0.33 s, roughly 10 times the pulse width of most pulsars. Even with this modest bandwidth and DM the smearing is sufficient to make the majority of pulsars undetectable and certainly prevents detailed study of the emission physics or pulse morphology.

Traditionally this problem has been solved by dividing the available bandwidth into narrower frequency channels, which are then delayed relative to each other by an amount dictated by the DM of the source. Because the maximum rate at which the data can be sampled is the inverse of the channel width, there is a limit to the number of channels one can divide a given bandwidth into, and thus at some point the resulting sampling time itself becomes too long. As pulsars are weak radio sources, large bandwidths are nonetheless required to improve the signal-to-noise ratio (S/N) of the detections. However until the advent of digital systems it was not possible to form the large number of channels required to use large bandwidths. A technique to fully correct for the effects of dispersion in the ISM was developed by Hankins (1971) but because it is computationally very expensive, this so-called coherent dedispersion has only seen regular use in the last 15 years or so. The strong dependence of dispersion on frequency has meant that coherent dedispersion has only seen limited use at low frequencies (e.g. Popov et al. 2006b; Karuppusamy et al. 2011). Until now the effect of dispersion has therefore been a strongly limiting factor on the number and types of pulsars which can be observed at low frequencies.

Furthermore, the ionised ISM is not distributed evenly and the inhomogeneities along a given line of sight between the Earth and a pulsar will cause the pulsed signal to take multiple paths, resulting in the pulse being scattered. Depending on the scattering regime, either strong or weak (Rickett 1990), along a particular sight line, the degree of temporal scattering of the pulse profile can scale as steeply as $\nu^{-4.4}$. Along a given line of sight it also shows a dependence on the total electron content, i.e. DM, but there are deviations from this relation of at least an order of magnitude (Bhat et al. 2004). Considering the same pulsar and observing frequecy and system as discussed in the first paragraph of this section, and using the relation between dispersion measure and scattering from Bhat et al. (2004) we find that the scattering delay would lie between 0.01 and 1 s. The stochastic nature of scattering means that it is difficult to uniquely correct for it without an underlying assumption for the intrinsic pulse shape; thus, scattering becomes the limiting factor on the distance out to which low-frequency observations can be used for detailed study, or even detection, of pulsars of given rotational periods.

3.2. Galactic background

Diffuse radio continuum emission in our Galaxy at frequencies below a few GHz is predominantly due to synchrotron emission from cosmic rays moving in the Galactic magnetic field. This emission has a strong frequency dependence ($\nu^{-2.6}$, Lawson et al. 1987; Reich & Reich 1988) and can thus be a significant component, or even dominate, the system temperature, $T_{\rm sys}$, at low frequencies. We note however that this spectral index does vary over the sky and especially in the low band it may turn over (Roger et al. 1999). Moreover, as the effect of the sky temperature on sensitivity can have a frequency dependence that is steeper than that of the flux density of some pulsars, pulsars located in regions of bright synchrotron emission, such as along the Galactic plane, become more difficult to detect at low radio frequencies. This is especially relevant as two-thirds of all known pulsars are found within 5° of the Galactic plane.

3.3. Ionosphere

LOFAR operates at frequencies just above the Earth's ionospheric cutoff, below which radio waves from space are reflected[3]. In this regime, the ionosphere still plays an important role in observations by contributing an additional time and frequency dependent phase delay to incoming signals. In particular, separate ionospheric cells can cause differential delays across the extent of an interferometric array like LOFAR, greatly complicating the calibration needed to add the signals from multiple stations together in phase. For a more detailed discussion of the ionosphere and LOFAR see Intema (2009) and Wijnholds et al. (2010a) and references therein. The specifics of the challenge for beam formed observations is described in greater detail in Sect. 6.

3.4. Addressing these challenges with LOFAR

The flexibility afforded by the almost fully digital nature of the signal path and the associated processing power of LOFAR mean that it can address these observational challenges better than any previous low frequency radio telescope. As will be discussed in Sect. 6 it is possible to take the complex channelised data

[3] Low-frequency radio frequency interference is also reflected back to Earth by the ionosphere and could potentially be detected from well below the local horizon.

coming from the LOFAR stations and either further channelise to achieve the required frequency resolution to correct for dispersion, or, when higher time resolution is required, it is possible to perform coherent dedispersion on the complex channels. While it is not presently possible to correct for the effects of scattering, we note that variations in the magnitude of scattering are so large that some pulsars with high DMs will still be accessible, as evidenced by our detection of PSR B1920+21 with a DM of 217 pc cm^{-3} (Fig. 4).

The system temperature of LOFAR is sky dominated at nearly all frequencies and when combined with the very large collecting area this makes LOFAR very sensitive despite the contribution from the Galactic synchrotron emission. The Galactic plane is clearly the hottest region, but that is only a small fraction of the sky[4] and as we are most sensitive to the nearby population it will not greatly affect the number of new pulsars LOFAR will find (see Sect. 4). Our detection of PSR B1749−28 (Fig. 4), which is only ∼1° from the direction to the Galactic Centre shows that observations of bright pulsars are still possible even with the large background temperature of the Galactic plane. Moreover, for observations of known pulsars in the direction of the Galactic plane, the narrow tied-array beams (see Sect. 5) will reduce the contribution from discrete extended sources, such as supernova remnants (SNRs), to the system temperature and thus further improve the sensitivity over single dish or wide beam telescopes.

In terms of calibrating the station/time/frequency dependent ionospheric phase delays, we will exploit LOFAR's multi-beaming capability and its ability to simultaneously image and record high-time-resolution pulsar data (Sect. 5). The envisioned scheme is to use a separate station beam to track a calibration source during an observation, use this to calculate the required phase adjustments per station, and to implement these online while observing the main science target with another beam. This is admittedly a difficult problem and the solution has yet to be implemented. In the case of the innermost core stations on the Superterp however, differential ionospheric delays are unlikely to be a major problem. This means that using the static phase solutions these stations can be combined coherently without ionospheric calibration.

4. Pulsar science at low frequencies

Here we give an overview of the pulsar science that can be done at low radio frequencies with LOFAR. This is not intended as an exhaustive list of envisioned studies, but rather as a general scientific motivation for LOFAR's pulsar modes.

4.1. Pulsar and fast transient searches

There are estimated to be approximately 100 000 actively radio-emitting neutron stars in the Milky Way (Vranesevic et al. 2004; Lorimer et al. 2006; Faucher-Giguère & Kaspi 2006), of which at least 20 000 are visible as radio pulsars due to fortuitous geometrical alignment of the radio beam with the direction towards Earth. With a sample of close to 2000 known radio pulsars to study, we still have only a rough idea of this population's overall properties and of the detailed physics of pulsars (Lorimer et al. 2006). This uncertainty is partly a product of the difficulty in disentangling the intrinsic properties of the population from the observational biases inherent to past surveys, most of which were conducted at ∼350 MHz or ∼1.4 GHz[5]. Discovering a large, nearby sample of pulsars with LOFAR will allow the determination of the distribution of pulsar luminosities in the low-luminosity regime, crucial for extrapolating to the total Galactic population, with the potential for detecting a cut-off in that distribution. Such a survey will also quantify the beaming fraction, that is what fraction of the sky is illuminated by the pulsar beams, at low frequencies, showing how this evolves from the more commonly observed 350/1400-MHz bands. Though a LOFAR pulsar survey will of course also be observationally biased towards a particular subset of the total Galactic pulsar population, these biases are in many ways complementary to those of past surveys, providing the opportunity to fully characterise the known population.

Detailed simulations of potential LOFAR surveys were done by van Leeuwen & Stappers (2010) and show that an all-Northern-sky survey with LOFAR will find about 1000 new pulsars and will provide a nearly complete census of all radio-emitting neutron stars within ∼2 kpc. An indication of the sensitivity of LOFAR for pulsar surveys can be seen in Fig. 2. The limiting distance out to which pulsars can be detected is governed predominantly by scattering in the ISM. There are however both pulsar and telescope characteristics that make low frequency surveys an attractive prospect. The pulsar beam broadens at low frequencies (Cordes 1978, find that the width changes with frequency ν as $\nu^{-0.25}$), which nearly doubles the beaming fraction compared to 1.4 GHz surveys. Furthermore, the large FoV and high sensitivity of LOFAR mean that such a survey can be carried out far more quickly and efficiently than any other pulsar survey, past or present. Even in the Galactic plane, where the diffuse background temperature will reduce the sensitivity, the ability to form narrow tied-array beams (see Sect. 5) will reduce the contribution from sources which are large enough to beresolved.

The large FoV also affords relatively long dwell times, improving the sensitivity to rare, but repeating events like the pulses from RRATs (rotating neutron stars which emit approximately once in every 1000 rotations, McLaughlin et al. 2006), while the rapid survey speed will allow multiple passes over the sky. Thus, such a survey is guaranteed to have a large product of total observing time and sky coverage ($\Omega_{\rm tot} T_{\rm tot}$). This factor is important for finding neutron stars that, for intrinsic or extrinsic reasons, have variable detectability, such as the RRATs and intermittent pulsars (the latter can be inactive for days: Kramer et al. 2006), those in relativistic binaries (where the acceleration near periastron can alter the periods too rapidly to allow detection (e.g., Johnston & Kulkarni 1991; Ransom et al. 2003), and those millisecond pulsars, MSPs[6], which are found in eclipsing systems (e.g., Fruchter et al. 1988; Stappers et al. 1996). It has recently become apparent that to understand the pulsar and neutron star populations we need to know what fraction of pulsars are relatively steady emitters compared with those that pulse erratically like the RRATs.

This complete, volume-limited sample can be extrapolated for modelling the entire neutron star population of the Galaxy, which then constrains the population of massive stars and the

[4] Note however that LOFAR's complex sidelobe pattern means that the Galactic plane can still contribute somewhat to the total sky temperature even for observations far from the plane itself.

[5] Reconciling the total number of neutron stars and the supernova rate (Keane & Kramer 2008) also remains an outstanding, related issue, with many fundamental questions still unanswered.

[6] MSPs are believed to be formed in binary systems, where the neutron star accretes matter from the companion star and is spun up to millisecond periods, sometimes referred to as recycling.

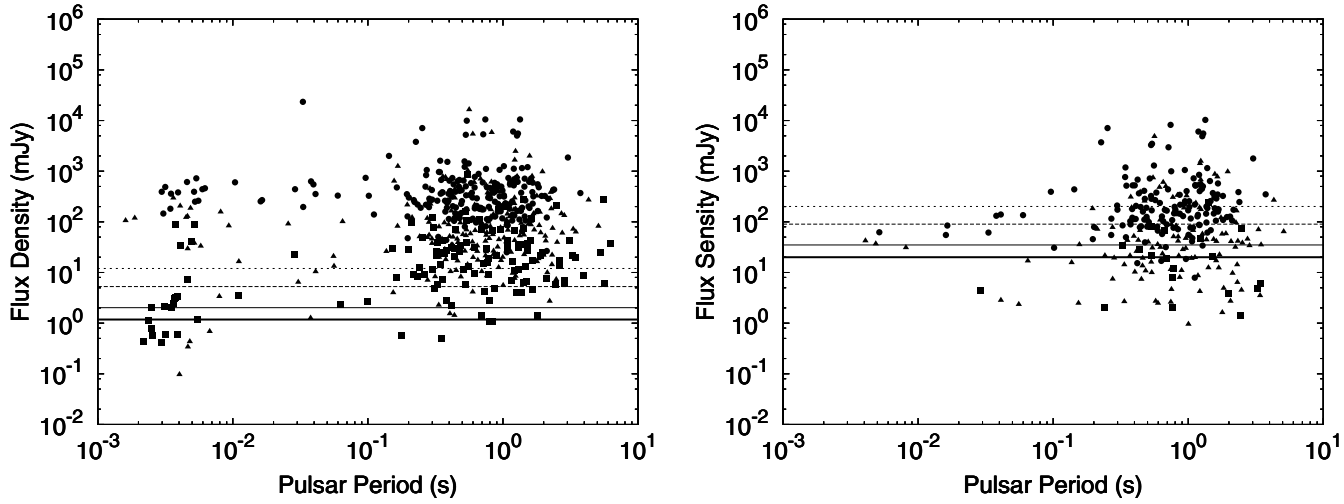

Fig. 2. Sensitivity curves for 600-s observations using the HBAs (*left*) and the LBAs (*right*) with a bandwidth of 48 MHz, compared to the extrapolated flux densities of 787 known pulsars at 150 and 50 MHz respectively. Flux densities were determined using, if known, 100 MHz fluxes from Malofeev et al. (2000) (circles) otherwise fluxes at either 400 MHz (triangles) or 1400 MHz (diamonds) (Manchester et al. 2005), whichever were available, were used and scaled to 150 MHz using a known spectral index or a typical spectral index of −1.8 (squares). All of these flux densities were scaled by $\sqrt{W/(P-W)}$, where W is the effective pulse width and P is the period of the pulsar, to incorporate broadening of the profile by scattering in the ISM. W was determined by combining the pulse width at high frequencies with the broadening due to scattering in the ISM, based on the model of Bhat et al (2004). If $W > 0.75P$ then the pulsar was deemed undetectable. It was assumed that broadening of the profile due to uncorrected dispersive smearing was negligible. MSPs are shown by the open symbols and "normal" pulsars by filled symbols. The lines in both cases correspond to the sensitivity of a single international station (fine dashed line), the incoherent sum of 20 core stations (heavy dashed line), incoherent sum of all LOFAR stations (filled line) and the coherent sum of 20 core stations (bold line).

supernova rate, the velocities and spatial distribution of neutron stars, and the physics of neutron stars in general. Chances are that this largely unexplored population of faint or intermittent radio-emitting neutron stars will also contain exotic systems – double neutron stars, double pulsars and possibly even a black-hole pulsar binary. Such systems provide the best testing ground for fundamental physical theories, ranging from solid-state to gravitational physics (Cordes et al. 2004a).

LOFAR is highly sensitive to MSPs and as they are generally much older than other neutron stars, they have had more time to leave their birth-place in the Galactic plane and to become equally distributed in the halo as well as in the plane. Thus, despite being more easily affected by scattering, the lower number of free electrons along the lines of sight out of the Galactic plane means that MSPs are still prime targets for LOFAR. Moreover, they are bright at LOFAR frequencies with the flux density spectra of some MSPs remaining steep down to 30 MHz (Kuzmin & Losovsky 2001; Kramer et al. 1999). Recent studies have successfully detected about half of the known Northern MSPs using the relatively insensitive low-frequency (110–180 MHz) frontends on the WSRT (Stappers et al. 2008). Malov & Malofeev (2010) have also shown a number of detections at frequencies near 100 MHz using the Large Phased Array BSA radio telescope of the Pushchino Radio Astronomy Observatory despite the limited time resolution. It is also noteworthy that the recently discovered "missing-link" MSP J1023+0038 (Archibald et al. 2009), detected with WSRT at 150 MHz, could have easily been found by a LOFAR survey, assuming it was observed out of eclipse. The number of MSPs uncovered at radio wavelengths, often at 350 MHz, by observations of unidentified *Fermi* sources (e.g. Ransom et al. 2011; Hessels et al. 2011) indicates that there are still many more relatively bright sources to be found. The high sensitiviy of LOFAR will allow it to detect nearby low-luminosity MSPs and steep spectrum high-luminosity MSPs which are too far away to be detected at high frequencies.

LOFAR also has the sensitivity to discover the brightest sources in local group galaxies (van Leeuwen & Stappers 2010). If observed face-on and located away from the Galactic disk, the scatter broadening to pulsars in an external galaxy will be relatively low and thus a LOFAR survey will have high sensitivity for even rapidly rotating extragalactic pulsars. For a relatively close galaxy like M 33, LOFAR could detect all pulsars more luminous than ∼50 Jy kpc^2. Ten of the currently known pulsars in our own Galaxy have comparable luminosity (Manchester et al. 2005). There are at least 20 (dwarf) galaxies for which LOFAR will have good sensitivity to their pulsar population. Complementing searches for periodic signals, detecting the bursts of either giant or RRAT pulses can equally pin-point pulsars. In particular, the ultra-bright giant pulses could be visible in even more remote galaxies (McLaughlin & Cordes 2003). A survey for extragalactic pulsars would allow us to investigate if the bright end of the pulsar distribution in other galaxies differs from that of our Galaxy, and how that ties into galaxy type and star formation history. Such pulsars can also feed the understanding of the history of massive star formation in these galaxies and also, if sufficient numbers can be found, they can be used to probe the intergalactic medium and possibly constrain or measure the intergalactic magnetic field.

In addition to the discovery of bright pulses from pulsars in nearby galaxies, an all-sky LOFAR survey will also cast a wide net for other extragalactic and cosmological bursts (e.g. Fender et al. 2008; van der Horst et al. 2008; Lorimer et al. 2007). The large FoV of LOFAR means that only 1200/200 pointings of station beams are required to cover the full Northern Hemisphere with the HBAs/LBAs at central frequencies of 150 and 60 MHz respectively[7]. Through a dedicated pulsar/fast transient survey,

[7] Compare for instance with the 1.4 GHz Parkes Multibeam system, which requires of the order of 35 000 pointings to cover a similar area of sky.

and regular piggy-backing on the imaging observations of other projects, it will be possible to obtain an unprecedented $\Omega_{\rm tot} \times T_{\rm tot}$ figure of merit. For example, 8000 HBA observations of 1 hr each (roughly two year's worth of observations, assuming 50% observing efficiency) would provide 4 h of all-sky coverage, meaning that events with rates of only 6/day over the whole sky could be detected in such a data set. The parameter space of such rare bursts has never been probed with such high sensitivity. Moreover there are many options for performing wide angle rapid shallow searches for fast transients using either single stations, forming sub-arrays or forming 244 LBA station beams all at once.

LOFAR will also respond to high-energy X-ray/γ-ray or high-frequency radio triggers. Most high-energy events peak later in the radio, providing ample time to follow-up on such events. Dispersive delay, which can easily be 100s of seconds in the LOFAR low-band, may also aid in detecting the prompt emission of some bursts. Efforts are being made to reduce the setup time of a typical observation so that target of opportunity observations can begin quickly and automatically. Since LOFAR has no moving parts, repointing is only a matter of reconfiguring the delay corrections used in beamforming. The ultimate goal is to repoint to any location of the sky and begin new observations in just a few seconds.

4.2. The physics of pulsar radio emission

The sensitivity and frequency range of LOFAR opens up the low-frequency window to new studies of pulsar emission. It is precisely in the LOFAR frequency range where some of the most interesting changes in pulsar radio emission can be observed, including significant broadening of the pulse profile, presumably due to a "radius-to-frequency" mapping and deviations from this expected relation; changes in the shape of pulse profile components; and a turn-over in the flux density spectrum. The frequency range accessible by LOFAR is also where propagation effects in the pulsar magnetosphere are expected to be largest (e.g. Petrova 2006, 2008; Weltevrede et al. 2003). Therefore, simultaneous multi-frequency observations (see Figs. 15 and 16) are expected to reveal interesting characteristics of the pulsar magnetosphere, such as the densities and birefringence properties (Shitov et al. 1988), that will ultimately lead to a better understanding of the emission mechanisms of pulsars.

4.2.1. Pulsar flux densities and spectra

LOFAR's large fractional bandwidth is a big advantage for measuring the low-frequency flux densities and spectra of pulsars. As discussed in Sect. 5.3 it will be possible to use multiple stations to observe contiguously from 10 MHz to 240 MHz. With the ability to easily repeat observations, we can be certain to remove effects such as diffractive scintillation, which may have affected previous flux density estimates. It is also the case that the timescale for refractive scintillation becomes very long at these frequencies and this will have a modulating effect on the determined fluxes. However this is typically of smaller amplitude. Repeating these observations will also allow one to determine whether the spectral characteristics are fixed in time, or whether they vary, for any given source, something which has rarely been done in the past. It is also important to note the role that variable scattering might play in flux density determination (e.g. Kuzmin et al. 2008).

So far, there are relatively few pulsars for which spectral information in the LOFAR frequency range is available (Malofeev et al. 2000). Obtaining a large, reliable set of low-frequency flux density measurements over the 4 lowest octaves of the radio window is a valuable missing piece in the puzzle of the pulsar emission process. For instance, the generally steep increase in pulsed flux density towards lower frequencies is seen to turn over for a number of pulsars at frequencies between 100 and 250 MHz. However, the physical origin for this turn over is not yet clear. Conversely, there are a number of pulsars for which no such break in the spectrum has yet been seen and studies at lower frequencies are needed to locate this spectral break (Kuzmin & Losovsky 2001; Malofeev 2000). Furthermore, there is evidence for complexity in the shape of pulsar spectra (e.g. Maron et al. 2000), which again is an important signature of the pulsar emission process that LOFAR's wide-band data can probe. In addition to their importance for our understanding of the emission process itself (e.g. Gurevich et al. 1993; Melrose 2004), pulsar spectra and flux densities are a basic ingredient for estimating the total radio luminosity and modelling the total Galactic population of radio pulsars.

In many ways, MSPs show very similar radio emission properties to those of non-recycled pulsars (e.g. Kramer et al. 1998); yet, they differ from these by many orders of magnitude in terms of their rotation period, magnetic field strength, and the size of their magnetosphere. A curious and potentially important distinction is that MSPs tend to show un-broken flux density spectra, continuing with no detected turn-over down to frequencies of 100 MHz (Kramer et al. 1999; Kuzmin & Losovsky 2001) and lower (e.g. Navarro et al. 1995). Kuzmin & Losovsky (2001) presented spectra of some 30 MSPs using measurements close to 100 MHz. Using the sensitivity, bandwidth and tracking abilities of LOFAR, it will be possible to more than double that number, and to provide measurements with much wider bandwidths. Such flux density measurements will also be possible using LOFAR's imaging ability, even if severe scattering prevents detailed profile studies. In general, however, when scattering is not the dominant effect the improved time resolution enabled by the coherent dedispersion mode of LOFAR should also allow us to resolve individual profile components in MSP profiles, so that the average profile spectrum can be compared to that of single pulse components.

Correlating the spectral properties with other properties of the pulsar (such as pulse shape, geometrical parameters or pulse energy distributions) may reveal important physical relationships. These can then be used to further improve pulsar emission and geometry models. This is particularly important as more and more sources are being detected at high energies with *Fermi*, placing interesting constraints on the emission sites (e.g. Abdo et al. 2010b).

4.2.2. Pulse profile morphology

Observations of the average pulse profile morphology of about 50% of pulsars studied over a wide frequency range indicate substantial and complex variations which are not easily understood in the standard model of pulsar emission (e.g. Lyne & Smith 2004; Lorimer & Kramer 2005). This simple pulsar model has the plasma and emission properties dominated by the dipolar magnetic field and is often combined with a model where the emission obeys a "radius-to-frequency mapping", such that lower frequencies are emitted further out in the magnetosphere resulting in wider pulse profiles (Cordes 1978). However this simple picture is not the full story as evidenced

by the spectral behaviour of the different pulse components (e.g. Mitra & Rankin 2002; Rankin 1993). The latter property is in general supported by observations, and probably corresponds to stratification of the density in the emission zone although plasma propagation effects may play an important role here as well (see e.g. Lorimer & Kramer 2005, for a review). The sensitivity and time resolution possible with LOFAR, combined with the wide frequency range, will allow us to obtain average profiles for the majority of the known population of pulsars in the Northern sky (Fig. 2). Additionally, hundreds of new pulsars, expected to be discovered with LOFAR, can also be studied in detail; as is demonstrated by the high quality data from our commissioning observations (Fig. 4).

There is also observational evidence that profiles that are dominated by the outer pulse components at high frequencies evolve to profiles where the central component is comparatively much stronger at low frequencies (e.g. Lorimer & Kramer 2005). The exact profile evolution may depend on the distribution of plasma along the field lines or may be the result of different emission zones. Indeed, the general picture is much more complex: variations are seen in the pulse profile with different components having different spectral indices and new components becoming visible (Kramer et al. 1994). By combining LOFAR data over its wide frequency range with higher frequency observations we can investigate these properties for a much larger group of pulsars (see for an example Fig. 16).

A further important probe of the emission mechanism, the geometry and the plasma properties of the magnetosphere is polarisation. So far, there have been only limited studies of the low-frequency polarisation properties of pulsars. In contrast, in simultaneous multiple high-frequency observations strange polarisation variations have been seen which point directly to the physics of the emission regions (e.g. Izvekova et al. 1994; Karastergiou et al. 2001). Polarisation studies with LOFAR have the potential to provide insight into how the polarisation behaves at these relatively unexplored low frequencies. LOFAR polarisation data can determine whether at low frequency the percentage of polarisation evolves strongly with frequency and if there are even more severe deviations of the polarisation position angle swing from the expectation for a dipole field. It will also be possible to determine if the polarisation properties change below the spectral break and whether the sign changes of circular polarisation seen at higher frequencies show similar properties at lower frequencies or exhibit no such sign changes.

4.2.3. Single pulses

The average, or cumulative, pulse profiles of radio pulsars are formed by adding at least hundreds of consecutive, individual pulses. While most pulsars have highly stable cumulative pulse profile morphologies, their individual pulses tend to be highly variable in shape, and require more complex interpretations than the average profiles. For example, single pulse studies of some pulsars have revealed quasi-periodic "micropulses" with periods and widths of the order of microseconds (Cordes et al. 1990; Lorimer & Kramer 2005). As such observed phenomena exhibit properties and timescales closest to those expected from theoretical studies of pulsar emission physics (e.g. Melrose 2004) studying them can strongly constrain models of the emission process. Single pulse studies at low frequencies are particularly interesting, because microstructure (Soglasnov et al. 1983; Smirnova et al. 1994) and subpulse modulation (Weltevrede et al. 2007; Ul'Yanov et al. 2008) tend to be stronger there. We also expect density imbalances and plasma dynamics to be the most noticeable at low radio frequencies (Petrova 2006).

In some pulsars, single sub-pulses are observed to drift in an organised fashion through the pulse window (see Fig. 13), an effect which may either be related to the creation of plasma columns near the polar cap or to the plasma properties within the pulsar magnetosphere. Some pulsars show significant frequency evolution in the properties of these drifting subpulses and observations at low frequencies, which probe a very different sight line across the typically enlarged emission beam, can be used to reconstruct the distribution of emission within the magnetosphere. Greater constraints can be obtained by simultaneous observations at different frequencies, within LOFAR bands but also in combination with high-frequency facilities. Such experiments will reveal how the radius-to-frequency mapping manifests itself in the sub-pulse modulation; for example, is the drifting more or less organised at the low frequencies? There is some evidence that drifting subpulses are more pronounced (Weltevrede et al. 2007) and perhaps easier to study at low frequencies.

In order to gauge the number of pulsars whose single pulses can be studied with LOFAR, we compare the estimated single-pulse flux densities in Fig. 3. We show all known pulsars visible with LOFAR and scale them to LOFAR sensitivity in both the high band and low band. While there are a number of assumptions (see caption of Fig. 3) that go into these calculations, we see that on average we expect to be able to see single pulses from about one third of visible pulsars in the high band and ten percent of visible pulsars in the low band. This is a significant increase on what has previously been possible. When combined with LOFAR's very wide bandwidth and the ability to track sources, it is clear that LOFAR will allow for a very rich study of the emission physics of radio pulsars (for example see Fig. 13). Based on the success of observing radio pulsars using multiple telescopes (e.g. Karastergiou et al. 2001, 2003; Kramer et al. 2003), we expect that in particular the combined simultaneous multi-frequency observations of single pulses at very low and high frequencies will be extremely useful in confirming or refuting some of the models and interpretations derived from previous data sets. The length and quality of the available data will be much improved, both by being able to follow sources for a much longer time than previously possible with low-frequency transit telescopes, and by having much better sensitivity, frequency coverage, and time resolution. In fact, LOFAR will also be able to detect single pulses from MSPs, something which has so far been done for only very few sources (Edwards & Stappers 2003; Jenet et al. 2001). This will allow us to study for the first time if pulsar phenomena discovered in normal, younger pulsars are also present in their much older brethren. Such effects include potential mode changing, nulling and drifting subpulse properties of MSPs. Understanding the occurrence of such effects will also be important for high precision timing at higher frequencies, as profile instabilities could, for example, hamper efforts to detect gravitational waves (Cordes & Shannon 2010). We note, however, that the high time resolution requirement of these observations compete with the effects of interstellar scattering which will ultimately limit the number of sources that can be studied. Nonetheless, we expect that a few hundred sources can be studied (Fig. 3), making this a particularly interesting aspect of pulsar studies with LOFAR.

4.3. Pulsars as probes of the ISM and the galactic magnetic field

Pulsars are ideal probes of the ionized component of the ISM, through the effects of scintillation, scattering, dispersion, and Faraday rotation. Most ISM effects become significantly

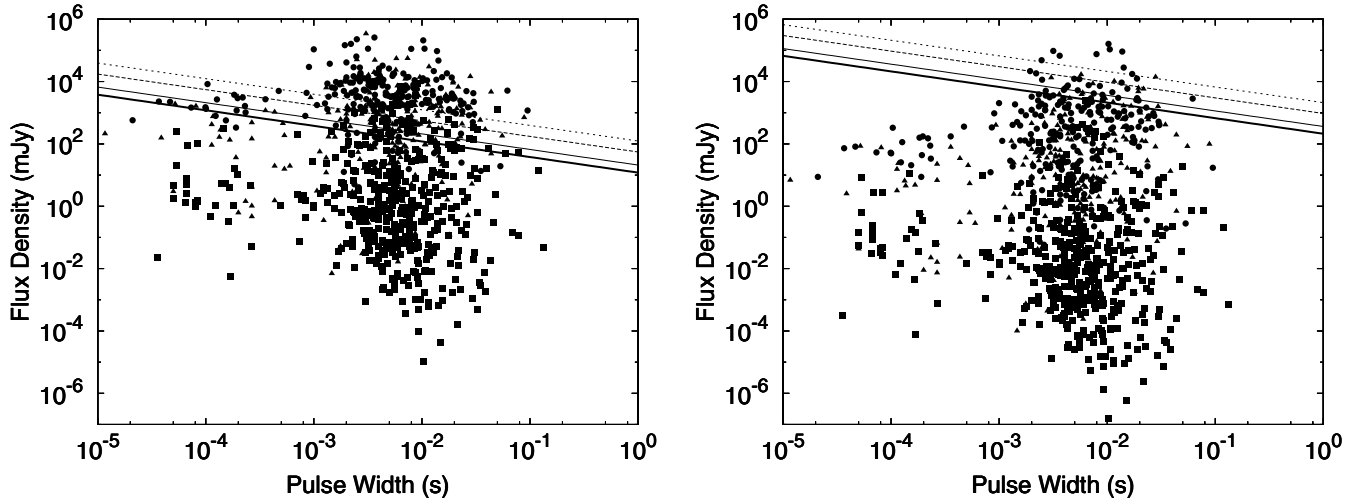

Fig. 3. Sensitivity curves for the HBAs (*left panel*) and LBAs (*right panel*) to single pulses as a function of pulse width at a central frequency of 150 MHz (HBAs) and 50 MHz (LBAs) and assuming a bandwidth of 48 MHz. Single pulse widths for 787 pulsars were calculated by assuming them to be one third of the width of the average pulse and then scatter broadened assuming the relationship of Bhat et al. (2004). It was assumed that broadening of the pulse due to uncorrected dispersive smearing was negligible. Single pulse fluxes were determined based on the assumed pulse width and, if known, 100 MHz fluxes from Malofeev et al. (2000) were used. Otherwise, fluxes were extrapolated to 150 MHz from either 400 MHz or 1400 MHz measurements (whichever was available, Manchester et al. 2005) using a known spectral index or a typical spectral index of −1.8. The symbols are the same as in Fig. 2. The lines in all cases correspond to the sensitivity of a single international station (fine dashed line), the incoherent sum of 20 core stations (heavy dashed line), incoherent sum of all the LOFAR stations (filled line) and the coherent sum of 20 core stations (bold line).

stronger towards low radio frequencies, meaning LOFAR is well placed to study these phenomena in the direction of known pulsars. Furthermore, by greatly increasing the number of known pulsars, a LOFAR pulsar survey will add a dense grid of new sight lines through the Galaxy. As the majority of these pulsars will be nearby or out of the Galactic plane, the dispersion and scattering measures of this new sample will improve our model of the distribution of the ionized ISM and its degree of clumpiness (Cordes & Lazio 2002).

Scintillation and scattering are related phenomena which result in variations of the pulse intensity as a function of frequency and time, and in broadening of the pulse profile respectively (e.g. Rickett 1970, 1990; Narayan 1992). They are caused by fluctuations in the density of free electrons in the ISM. Scintillation studies have been revolutionised in the last few years by the discovery of faint halos of scattered light, extending outward to 10–50 times the width of the core of the scattered image (Stinebring et al. 2001). This, in turn, gives a wide-angle view of the scattering medium with milliarcsecond resolution, and the illuminated patch scans rapidly across the scattering material because of the high pulsar space velocity. Some of the most interesting effects are visible at low frequencies. The dynamic nature of these phenomena also fits well with LOFAR's monitoring capabilities. In a sense, this scintillation imaging will allow the monitoring of the range of interstellar conditions encountered along a particular sight line. The wide bandwidths and high sensitivities will also allow very precise measurements of the DM of many pulsars; for MSPs this could be as precise as $1{:}10^4$ or better for an *individual* measurement. Such precision, even for normal pulsars, will enable detailed studies of variations in the DM which can be used with the scintillation properties to study structures in the ISM (e.g. You et al. 2007).

Scattering is a spatial effect, whereby the inhomogeneities in the ISM cause ray paths to be redirected into the line of sight with a resulting delay associated with the extra travel time. Scattering is typically assumed to happen in a thin screen located midway between the pulsar and the Earth, so that the turbulence obeys a Kolmogorov law even though deviations are observed (e.g. Löhmer et al. 2004). There is evidence that the scattering does not have the expected frequency dependence for such a spectrum and that there is also an inner and outer scale to the turbulence which can be measured (e.g. Armstrong et al. 1981, 1995; Shishov & Smirnova 2002). Low-frequency measurements with LOFAR will allow us to measure (even subtle) scattering tails for many more pulsars, affording better statistical studies. The study of individual, moderately scattered but bright pulsars will provide a probe of the distribution of electrons along the line of sight, enabling one to distinguish between the different frequency dependences of the dispersive and scattering delays that affect the arrival time of the pulse (see for example Fig. 19). Identifying such effects has the potential to extract distances and thicknesses of scattering screens (Rickett et al. 2009; Smirnova & Shishov 2010).

LOFAR can increase the number of known rotation measures to pulsars, which will place important constraints on the overall magnetic field structure of the Milky Way, something that is still not well characterised (e.g. Noutsos et al. 2008; Han 2009; Wolleben et al. 2010). At LOFAR frequencies it is possible to also measure the very small rotation measures of the nearby population of pulsars which provides an unprecedented tool for studying the local magnetic field structure. The large number of new sight lines will also allow statistical studies of small-scale fluctuations of electron density and magnetic field variations down to the smallest scales that can be probed with pulsars ($\lesssim$1 kpc). These same techniques will open up new vistas when applied to the first (truly) extragalactic pulsars, which will be discovered by LOFAR in the survey of local group galaxies that will be undertaken.

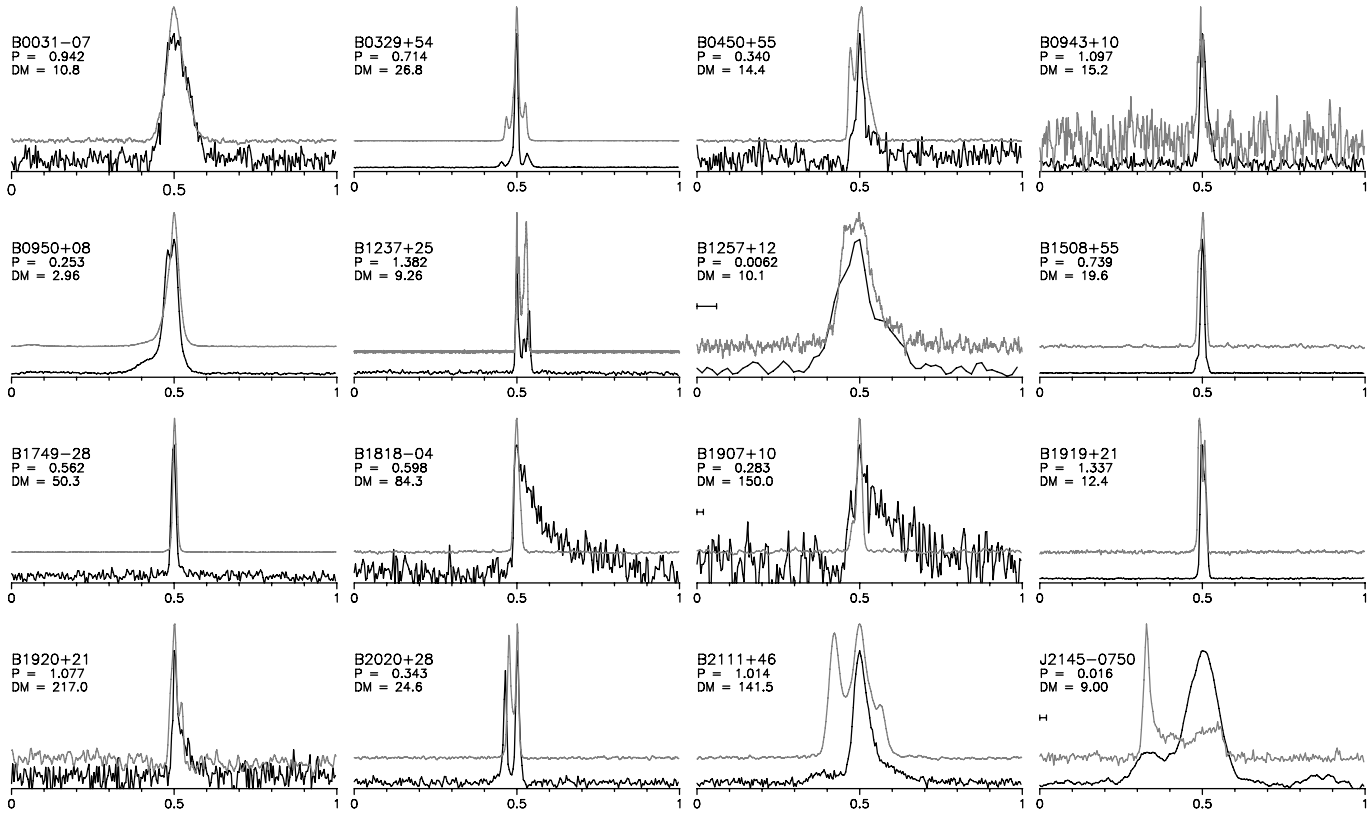

Fig. 4. A sample of average pulse profiles from LOFAR observations of various pulsars made during the commissioning period. The dark line corresponds to LOFAR observations made with the HBAs with 48 MHz of bandwidth, divided into 3968 channels, at a central frequency of 163 MHz. Typically about 12 stations were used and they were combined incoherently. The abcissa is the rotational phase and at present there is no flux calibration for the LOFAR data, hence no flux scale is shown. The majority of the observations are ∼1000 s in duration, except for PSR B1257+12, which was observed for 3 h. The dispersion measure smearing is less than two bins for the majority of the pulsars shown; if the smearing is large, this is indicated by a bar on the left hand side. The lighter line corresponds to observations made at 1408 MHz by Gould & Lyne (1998) except for the observations of PSR B0943+10 which was at 608 MHz and PSR B1237+25 which was at 1600 MHz (from van Hoensbroech & Xilouris 1997). All archival profiles are from the EPN database (`www.mpifr-bonn.mpg.de/div/pulsar/data/browser.html`); they are shown for illustration purposes and are manually aligned. Both the LOFAR and EPN profiles have been normalised to the peak intensity. The periods are given in seconds and the dispersion measures in pc cm^{-3}.

4.4. Pulsar timing

Ultra-high-precision pulsar timing (at the ns−sub-μs level) is not possible at low radio frequencies because the timing precision is strongly affected by ISM effects that, currently at least, cannot be compensated for. However LOFAR's large FoV, multi-beaming capability, and the availability and sensitivity of single stations working in parallel to the main array enable many pulsars to be timed at sufficient precision and cadence to be of scientific interest. Regular monitoring of the rotational behaviour of radio pulsars plays an important role in understanding the internal structure and spin evolution of neutron stars and how they emit. It is also an important probe of the ISM and potentially for the emission of gravitational waves. Measuring DM variations and modelling the scattering of pulse profiles at LOFAR frequencies has the potential to help correct pulse shape variations at high observing frequencies and thus reduce systematics in high precision timing.

Rotational irregularities such as glitches are attributed to the physics of the super-dense superfluid present in the neutron star core, and so their study allows us to probe a physical regime far beyond those that can be reached in laboratories on Earth (e.g. D'Alessandro 1996; van Eysden & Melatos 2010). These glitches might also trigger heating of the neutron star surface or magnetic reconnections which can be studied in either or both gamma- and X-rays (Tang & Cheng 2001; Van Riper et al. 1991). They may also cause sufficient deformation of the neutron star that it might be a gravitational wave emitter (e.g. Bennett et al. 2010). To allow these multi-messenger follow-up observations requires the accurate determination of glitch occurence times which can be achieved through regular monitoring with LOFAR. Moreover, the studies of high-energy emission from pulsars, which is presently done in detail by the *Fermi* and *Agile* satellites and other telescopes like MAGIC and H.E.S.S. (e.g. Abdo et al. 2009; Tavani et al. 2009; Aliu et al. 2008; Aharonian et al. 2007), as well as the search for non-burst-like gravitational waves from pulsars (Abbott et al. 2010) can only be performed with the provision of accurate pulsar rotational histories.

Three relatively recently discovered manifestations of radio emitting neutron stars, the RRATs, the intermittent pulsars, and the radio emitting magnetars (McLaughlin et al. 2006; Kramer et al. 2006; Lyutikov 2002; Camilo et al. 2006), can all greatly benefit from the monitoring capabilities of LOFAR. All of these source types show only sporadic radio activity, which in some cases is only present for less than a second per day. As such, a large amount of on-sky observing is often preferable to raw sensitivity, making such studies particularly well-suited for individual LOFAR stations observing independently from the rest of

the array. It is possible that there are neutron stars whose radio emission is even more sporadic; discovering these will require potentially several days of cummulative integration time per sky position, which is achievable as part of the LOFAR Radio Sky Monitor (Fender et al. 2008).

So far some 30 RRATs have been discovered, though periods and period derivatives have only been determined for slightly more than half of these (McLaughlin et al. 2009). Detailed studies of these sources are hampered by the fact that they pulse so infrequently as to make proper timing follow-up prohibitively expensive for most telescopes. LOFAR's multi-beaming capabilities and the separate use of single stations make such studies feasible. These can determine key parameters like the spin period $P_{\rm spin}$ and its derivative $\dot{P}_{\rm spin}$ as well as better characterising the nature of the pulses themselve. These are all essential for understanding the relationship of RRATs to the "normal" pulsars.

Unlike the RRATs, the intermittent pulsars appear as normal pulsars for timescales of days to months, but then suddenly turn off for similar periods (Kramer et al. 2006). Remarkably, when they turn off they spin down more slowly than when they are on, providing a unique and exciting link with the physics of the magnetosphere. Observing more on/off transitions will improve our understanding of the transition process. Furthermore, recent work by Lyne et al. (2010) has shown similar behaviour in normal pulsars, relating timing noise, pulse shape variations and changes in spin-down rate. Moreover they demonstrate that with sufficiently regular monitoring, that can be achieved with telescopes like LOFAR, it may be possible to correct the effects these variations cause on the pulsar timing. This will allow for the possibility of improving their usefulness as clocks.

Another manifestation of radio pulsars which show highly variable radio emission are the magnetars, extremely magnetised neutron stars ($B_{\rm surf} \sim 10^{14-15}$ G), which were thought to emit only in gamma- and X-rays. Recently, however, two such sources have been shown to emit in the radio, albeit in a highly variable way (Camilo et al. 2006, 2007). This emission may have been triggered by an X-ray burst, and was subsequently observed to fade dramatically. Even more recently, a radio pulsar was discovered which has a rotation period and magnetic field strength within the observed magnetar range. This pulsar also shows similarly variable radio emission properties, as seen for the other two "radio magnetars", though no X-ray burst has been observed (Levin et al. 2010). It is only by monitoring these sources, and regularly searching the sky, in the radio that we can understand the link between intermittent radio pulsations and high-energy bursts, as well as the lifetime of these sources as radio emitters.

4.5. New populations

The case for observing pulsars at low frequencies, as discussed so far, is partly based on our knowledge of the typical spectral behaviour of the known population. However, there are pulsars like PSR B0943+10, which have flux density spectra with spectral indices steeper than $\alpha = -3.0$ (Deshpande & Radhakrishnan 1994) and a number of MSPs which have steep spectra and which do not show a turn-over even at frequencies as low as 30 MHz (e.g. Navarro et al. 1995). It is as yet unclear whether these extreme spectral index sources represent a tail of the spectral index distribution. There is a potential bias against steep spectrum objects as they need to be very bright at low frequencies in order to be detected in high-frequency surveys. For example, the minimum flux density of the HTRU, High Time Resolution Universe, survey with the Parkes telescope at 1400 MHz (Keith et al. 2010) is 0.2 mJy and for a spectral index −3.0 pulsar the corresponding 140 MHz flux density would be 200 mJy. In contrast, a source close to the LOFAR search sensitivity of about 1 mJy would have to have a flux density no steeper than −0.7 to be detected by HTRU, suggesting that a large number of pulsars may only be detectable at low frequencies.

Beyond these regular pulsars with steep spectral indices, more exotic neutron stars are seen to show transient radio emission. While the anomalous X-ray pulsars XTE J1810-197 and 1E 1547.0-5408 (Camilo et al. 2006, 2007) have shallow spectral indices and are very dim in the LOFAR regime, several other AXPs and magnetars may appear to be only detectable at frequencies near 100 MHz (e.g. Malofeev et al. 2006), offering an intriguing possibility to study more of these high-magnetic-field objects in the radio band if confirmed. The potential 100-MHz detection of Geminga, a prominent rotation-powered pulsar visible at optical, X-ray and gamma-ray wavelengths (Malofeev & Malov 1997; Kuzmin & Losovskii 1997; Shitov & Pugachev 1997), could exemplify a population of neutron stars that may be only detectable at radio wavelengths with LOFAR. Also, the non-detection of radio emission from X-ray dim isolated neutron stars (XDINSs) thus far (Kondratiev et al. 2009), could be due to the beams of these long-period sources being quite narrow at high frequencies and there may be a better chance to detect them in radio at LOFAR frequencies. In fact, weak radio emission from two XDINSs, RX J1308.6+2127 and RX J2143.0+0654, was reported by Malofeev et al. (2005, 2007) at 111 MHz, hence it would be important to confirm this detection with LOFAR. This is also the case for the pulsars discovered in blind searches of *Fermi* gamma-ray photons, many of which do not exhibit detectable radio emission (Abdo et al. 2009, 2010b), as well as the remaining unidentified gamma-ray sources, which have characteristics of radio pulsars but which have not yet been detected in the radio (Abdo et al. 2010a).

5. Observing modes

Here we describe LOFAR's various "beamformed" modes, both currently available or envisioned, for observing pulsars and fast transients. Though we concentrate on the pulsar and fast transient applications of these modes, we note that LOFAR's beamformed modes are also applicable to other high-time-resolution studies including dynamic spectra of planets (both solar and extra-solar), flare stars, and the Sun. We also provide a brief description of LOFAR's standard interferometric imaging mode, which can be run in parallel with some beamformed modes. For a detailed description of LOFAR imaging, see Heald et al. (2010) and van Haarlem et al. (in prep.).

LOFAR is an interferometer with sparsely spaced stations, distributed in such a way as to produce reliable high-resolution images. To achieve this, the data from all stations are correlated[8] with each other, resulting in a significant increase in the amount of data. To reduce the data rate to an acceptable level there is an averaging step which reduces the time resolution of the data to typically about one second, or longer (though somewhat shorter integrations are possible in some cases). To sample the combined radio signal at significantly higher time resolution than this ($t_{\rm samp} < 100$ ms), one has to normally sacrifice spatial resolution, and/or the large FoV seen by the individual elements, to form a single beam pointing in the direction of the source of interest. It is these so-called beamformed or pulsar-like modes that we will describe here. The LOFAR Transients Key Science

[8] Note that the antennas within an individual station are first summed in phase to form one or multiple station beams on the sky.

Table 3. Comparison of the LOFAR beam-forming modes.

Mode	Sensitivity (Norm.)	FoV (sq. deg)	Resolution (deg)	Data rate (TB/h)	FoM (Norm.)
High-Band Antennas (HBAs)					
Single HBA sub-station	1/0.35	18/147	4.8	0.3	1
Single Rem. Station	2/0.7	10/82	3.6	0.3	3
Single Intl. Station	4/1.4	6 /45	2.7	0.3	9
Fly's Eye	1/0.35	1050/8400	4.8	20	56
Dutch Inc. Sum	11/4	10/82	3.6	0.3	77
Intl. Inc. Sum	11/4	6/45	2.7	0.3	73
Coherent Superterp (94 beams)	12/4	18/147	0.5	29	1382
Coherent Sum Core (100 beams)	48/17	0.4/3	0.075	31	3206
Constrained Coherent Core (29 beams)	10/3.5	18/147	0.9	9	512
Low-Band Antennas (LBAs)					
Single Core Station Outer	1/0.35	17/132	4.6	0.3	1
Single Core Station Inner	<1/<0.35	105/840	11.6	0.3	<1
Single Rem. Station	1/0.35	17/132	4.6	0.3	1
Single Intl. Station	2/0.7	26/211	5.8	0.3	5
Fly's Eye	1/0.35	660/5300	4.6	12	40
Dutch Inc. Sum	6/2	17/132	4.6	0.3	40
Intl. Inc. Sum	6/2	26/211	5.8	0.3	44
Coherent Superterp (15 beams)	6/2	17/132	1.2	4.5	138
Coherent Sum Core (100 beams)	24/8.5	3/23	0.19	30	2460

Notes. LOFAR beam-formed modes and their (approximate) associated sensitivity, FoV, resolution (i.e. $\Delta\Omega$), data-rate, and survey FoM (see text). High-band (HBA) and low-band (LBA) sensitivities and FoMs have been normalized to that of a single 24-tile HBA sub-station or a 48-dipole Dutch LBA field respectively (Recall that each Dutch LBA field contains 96 dipoles, only 48 of which are used in any particular observation. Unless otherwise stated, we assume the LBA Outer mode is being used. This mode gives somewhat higher gain, but reduced FoV compared with the LBA Inner mode.). Quantities are quoted assuming one beam per station (48 MHz bandwidth) and 8 beams per station (6 MHz bandwidth per beam) respectively. FoV ($\propto\lambda_{\rm obs}^2$) and resolution (i.e. *FWHM* of the beam, $\propto\lambda_{\rm obs}$) are quoted for a central observing frequency of 150 MHz (HBA, $\lambda_{\rm obs}$ = 2 m) and 60 MHz (LBA, $\lambda_{\rm obs}$ = 5 m). Note that *FWHM* is taken to be $\alpha \times \lambda_{\rm obs}/D$, where α = 1.3 and D is the size of a station or the maximum baseline between combined stations where applicable. As LOFAR stations consist of several square tiles, they are not perfectly circular; thus, the product of FoV and sensitivity is not constant when station size increases. We have used LBA (Inner)/LBA (Outer)/HBA station sizes of 32.3 m/81.3 m/30.8 m (core), 32.3 m/81.3 m/41.1 m (remote), and 65 m/56 m (international, Inner/Outer mode does not apply here). Further empirical beam modeling will likely refine the value of α, and will somewhat effect the rough values quoted here. Where applicable, we assume that 24 core stations of 2×24 HBA tiles/48 LBA dipoles, 16 Dutch remote stations of 48 HBA tiles/48 active LBA dipoles, and 8 international stations of 96 HBA tiles/96 LBA dipoles are available and can be recorded separately if desired. Fly's Eye mode assumes all Dutch stations – i.e. 48 HBA core sub-stations plus 16 remote HBA stations or 40 LBA fields of 48-dipoles each are used. For the "Coherent" modes, we assume the maximum number of tied-array beams required to cover the station beam, up to a maximum of 100 (per station beam), can be synthesized, and that the maximum baseline between stations is 300 m for the Superterp and 2000 m for the entire Core. The "Coherent Sum Core" mode assumes that all 48 Core sub-stations are combined coherently. The "Dutch Incoherent Sum" mode assumes that all 40 Dutch stations (24 core/16 remote) are combined incoherently. The "Intl. Incoherent Sum" mode assumes that all 8 international stations are combined incoherently. The "Constrained Coherent Core" mode is a hybrid coherent/incoherent summation in which the two HBA sub-stations of each core station are first summed coherently at station level before these stations are in turn summed incoherently. The integration time used in each mode is assumed to be the same, though this would likely differ in practice, especially in the case of wide-field surveys. The data rates assume 16-bit samples (this could be reduced if desired), summed to form Stokes I, at the maximum possible spectral/time resolution, which for certain applications can be downgraded by a factor of a few in order to save on disk space and processing load.

Project (Fender et al. 2006) will use both the imaging and beam-formed modes to discover and study transient sources. The imaging mode will probe flux changes on timescales of seconds to years, while the beamformed modes will probe timescales from seconds down to microseconds and will revisit the same sky locations over the course of days to years. With the Transient Buffer Boards (TBBs; Sect. 5.5) it will be possible to form images with high time resolution, but limited observing durations.

There are many ways in which the various parts of LOFAR (antennas, tiles, stations) can be combined to form beams (see Table 3). The almost completely digital nature of the LOFAR signal processing chain means that it is highly flexible to suit a particular observational goal. In the following sub-sections we will discuss different options for combining these signals, to maximise either the FoV, instantaneous sensitivity or to compromise between these two factors. For the sake of clarity however, we begin by defining some related terms. An *element beam* refers to the FoV seen by a single element, a dipole in the case of the LBAs and a tile of 4×4 dipoles in the case of the HBAs (recall that these dipoles are combined into a tile beam using an analog beamformer). The term *station beam* corresponds to the beam formed by the sum of all of the elements of a station. For any given observation there may be more than one station beam and they can be pointed at any location within the wider element beam. A *tied-array beam* is formed by coherently combining all the station beams, one for each station, which are looking in a particular direction. There may be more than one tied-array beam for each station beam. Station beams can also be combined

incoherently in order to form *incoherent array beams*. These retain the FoV of the individual station beams and have increased sensitivity compared with a single station.

5.1. Coherent and incoherent station addition

5.1.1. Coherent addition

To achieve the full sensitivity of the LOFAR array it is necessary to combine the signals from each of the station beams coherently, meaning that the phase relationship between the station signals from a particular direction must be precisely determined. Phase delays between the signals are generated by a combination of geometric, instrumental, and environmental effects. The geometric term is simply related to the relative locations of the stations and the source and is easily calculated. Instrumental contributions are related to the observing system itself, such as the length of cables connecting the various elements. Consequently, the components in the signal chain are designed to be stable on timescales that are long compared to the observing duration. The environmental terms can be much more variable and are dominated by ionospheric delays at low radio frequencies.

Combining the station signals coherently into tied-array beams gives the equivalent sensitivity to the sum of the collecting area of all the stations being combined. However, the resulting FoV is significantly smaller than that of an individual station beam because it is determined by the distance between stations, which for LOFAR is significantly larger than the size of the stations themselves. The FoVs for various beam types are given in Table 3 and examples are shown in Fig. 1. The small FoV of tied-array beams is not a problem for observing known point sources – in fact, it can be advantageous by reducing the contribution of background sources – but increases the data rate and processing requirements when undertaking surveys (see below).

The coherent combination of telescopes for pulsar observations is regularly used at the Westerbork Synthesis Radio Telescope (Karuppusamy et al. 2008) and the Giant Meter-Wave Radio Telescope (Gupta et al. 2000). In both cases the phase delays between the telescopes are determined by regular observations of known and unresolved calibration sources in a process which is often called "phasing-up". The timescale between when observations of calibration sources need to be made depends strongly on the observing frequency, the largest separation between telescopes and the ionospheric conditions, but range from a few hours to days.

At the low frequencies of LOFAR, phase delays between stations are very susceptible to the influence of ionospheric disturbances (e.g. Nijboer & Noordam 2007). This directly affects how often phasing-up needs to be done, as well as the maximum separation between stations that can be coherently combined. Fortunately, LOFAR's flexible signal processing provides a number of options to rapidly phase-up (at least) those stations located in the core (the innermost 2 km of the array). The first option makes use of LOFAR's ability to produce images in near real time. As part of the imaging calibration, the phase delays between stations are determined. As it is possible to operate imaging and beamformed modes simultaneously (see also Sect. 7.1.4) the phases from the imaging pipeline can be used to coherently combine the stations, and to update the calibration continuously. If for some reason this isn't sufficient, a second option is available in which it is possible to trade a small amount of observing bandwidth to form a station beam which points at a strong calibrator somewhere in the wide FoV of the element beam. As long as this probes a similar ionospheric patch, this can be used to monitor the phases.

An important aspect of keeping the signals from the stations in phase is the time stamp given to each sample. In the original design, LOFAR used separate rubidium clocks at each of the stations. These clocks in turn are governed by their own Global Positioning System receiver, which steers the rubidium clock drifts to maintain long-term timing stability. However it was recognised that while the instantaneous accuracy was sufficient, there were medium term drifts which needed to be corrected for. To alleviate the need for such corrections on the LOFAR Superterp, a new single clock system has been implemented: the clock signal from one GPS-governed rubidium clock is distributed to these 6 stations. The rest of the core stations will be kept in phase for the coherent addition using either of the two methods described above.

Once the phase delays have been determined between the stations, it is possible to use different geometrical delays to form additional tied-array beams. These additional tied-array beams can be used to tesselate sections of a single station beam, in order to greatly increase the total FoV for survey-like observations. They can also be formed inside different station beams to point at many different known point sources simultaneously, thereby greatly improving observing efficiency (see Fig. 1 for examples of beams). The processing capability of CEP will allow us to form at least 200 tied-array beams simultaneously, depending on the observing bandwidth and time resolution used. This allows LOFAR to achieve rapid survey speed despite the decrease in FoV caused by the wide distribution of the stations. Though the resulting data rate is very large, an advantage of surveying with tens to hundreds of tied-array beams is that the position of newly found sources is immediately known to an accuracy of $\sim 5'$ (when all core stations are used). This can save significant follow-up observation time that would otherwise be spent refining the source position.

5.1.2. Incoherent addition

It is also possible to combine the stations without correcting for the phase differences between them. If the signals are added after detecting them (i.e. computing the power and thereby losing the phase information) this results in a so-called incoherent sum. As there is no longer any phase relation between the signals from the stations, the signals do not constructively nor destructively interfere. The combined signal is therefore sensitive to signals anywhere within the FoV of the station beam, however the sensitivity increases only as the square-root of the number of stations combined.

As it is not necessary to keep track of the phase relationship between the stations, the incoherent addition can incorporate stations which are more widely spread than those that can be coherently combined. Determining which mode to use, for any given observing goal, depends on the amount of collecting area which can be combined coherently, the number of tied-array beams that can be formed and the science goals.

As previously discussed in Hessels et al. (2009) the observational requirements, e.g. sensitivity and FoV, can be distilled into a simple figure of merit (FoM, see Table 3), which is generally applicable to a transient survey[9](see also Cordes et al. 2004b;

[9] We choose to give extra weighting to $A_{\rm eff}$. One may also consider a FoM that scales linearly with $A_{\rm eff}$.

Cordes 2008, and references therein for a deeper discussion of survey metrics):

$$FoM \propto A_{\rm eff}^2 \frac{\Omega}{\Delta\Omega}\frac{T}{\Delta T}. \quad (1)$$

To be sensitive to transients over a wide range of source parameter space, including faint and rare events, this FoM should be maximized. This means maximizing: $A_{\rm eff}$, the effective collecting area being used; Ω, the instantaneous field of view (FoV); and T, the total time spent observing the sky. At the same time, adequate spatial ($\Delta\Omega$) and time (ΔT) resolution are needed to provide reasonable source localization, for multi-wavelength follow-up and identification, and to resolve short timescale phenomena. As it is not possible to maximize both raw, instantaneous sensitivity and FoV simultaneously, different modes naturally probe different areas of transient parameter space (see below).

5.1.3. Coherent versus incoherent addition for different science cases

Contingent on the particular science goals, pulsar and fast transient surveys with LOFAR are likely to be performed using both the coherent and incoherent addition modes, sometimes in parallel. As discussed by van Leeuwen & Stappers (2010), a high sensitivity survey of the entire Northern Sky is preferentially done using the coherent addition of stations if one can form at least ~200 tied-array beams[10]. Though such a mode provides the best-possible source localization and sensitivity, this comes at the price of a much larger data rate (Table 3) and consequently much greater processing requirements. In comparison, the wide FoV afforded by the incoherent sum gives it a very competitive survey speed. However, there are several drawbacks compared with the coherent mode: source localization is comparatively poor, as is the rejection of astronomical backgrounds and radio frequency interference (RFI). Also, in the incoherent modes much longer observing times are needed to achieve the same sensitivity and/or FoM (Table 3), which increases the processing load significantly if acceleration searches for binary systems are to be performed (e.g. Johnston & Kulkarni 1991; Ransom et al. 2003). On the other hand, longer dwell times may be advantageous for detecting certain types of transients. Nonetheless, the incoherent addition mode provides a way to rapidly survey the whole sky[11] with a competitive sensitivity, thereby making it very useful for detecting classes of pulsars which can emit relatively brightly but more erratically, e.g. RRATs, intermittent pulsars, radio emitting magnetars, and eclipsing sources, as well as other transient sources like flare stars, planets and potentially new classes of transient sources.

Observations of known point sources at high time resolution, where the maximum sensitivity over a given bandwidth is required, are best achieved by using the coherent sum mode. As discussed earlier, even in this mode multiple sources can be observed simultaneously if multiple station beams are used at the expense of total bandwidth. Each of the tied-array beams can be considered as an independent entity in the LOFAR processing chain and so, e.g., pulsar timing campaigns can be run efficiently by observing multiple sources at once. It is also possible to have beams pointing at a range of source types, for example a pulsar, a planet, a flare star, and an X-ray binary all at the same time, with different data products being produced for each of the different sources.

[10] Current system performance tests indicate that this should be achievable.

[11] Using 7 station beams per pointing, only about 200 HBA pointings are required to cover the entire LOFAR-visible sky ($\delta > -35°$).

5.2. Observing in multiple modes simultaneously

5.2.1. Coherent and incoherent sum modes

LOFAR is flexible enough to produce coherently and incoherently added data simultaneously. This provides, at the incoherent summation sensitivity, the full FoV of a single station while still having the full coherent sensitivity in the centre of the FoV. Though even 200 tied-array beams, generated using all the stations on the core, only cover ~3% of the single station FoV, this parallel mode allows one to both survey the sky at very high sensitivity (over a small FoV) and over a large FoV (at lower sensitivity) simultaneously (Table 3). We note that a greater fraction of the single station FoV can be covered if we coherently sum the Superterp stations only, and this may also prove a useful survey mode. Alternatively, a mix of coherent and incoherent addition can be used when adding the stations. For example, one might choose to coherently sum the stations in the compact core of the array, e.g. on the Superterp (Fig. 1), and then incoherently add the stations outside of the core to this. This results in a compromise between FoV and sensitivity because the core stations have relatively short baselines between them (Fig. 1). It also results in a more complex combined beam shape. In contrast, groups of stations can also be used separately as part of sub-arrays, as discussed below.

5.2.2. Imaging and beamformed modes

As mentioned above, beamformed data can be taken in parallel with imaging observations. This opens up the opportunity for commensal observing where searches for fast transients can take place in parallel with imaging-based searches for slow transients or other observations. This will be done as part of the Transient Key Science Project's Radio Sky Monitor, which will image the sky down to 1 s timescales; we will continuously record the incoherent sum of the stations to probe variability on even faster timescales. In Sect. 7.1.4 (Fig. 12) we present the first such simultaneous imaging/beamformed observation made with LOFAR taken in 2010 April, when only 7 LOFAR stations were available for imaging.

5.3. Observing with sub-arrays and single stations

In addition to the incoherent and coherent modes of observing described above, the array can be split up in various flexible ways to accommodate particular science goals. There are certain pulsar and fast transient science goals with observational requirements that are best served by grouping the stations into sub-arrays, or using individual stations independently. In this way, sensitivity can be exchanged for a larger total FoV and/or broader total frequency coverage.

For large sky coverage, LOFAR sub-arrays consisting of one or several stations (depending on the required sensitivity) can be used to point at different directions, covering a large fraction of the sky – potentially the *entire* LOFAR-visible sky in the case of the LBAs (Table 3). To maximize FoV, each sub-array can simply be a single station pointing in a unique direction. This mode, referred to as Fly's Eye, is very similar to that developed for the Allen Telescope Array (ATA, Welch et al. 2009) and will be used to monitor for rare, very bright, fast transient events. In this mode

the localization of detected bursts can only be achieved to within the single station FoV, which ranges from a few square degrees to many hundred square degrees across the LOFAR band. Much better position determination could be achieved by triggering as the source is detected and then using the TBBs to subsequently image the sky to try to find the source (see Sect. 5.5 for more details).

Another option involves using sub-arrays of stations tuned to complementary frequencies across the entire LOFAR band, pointing at the same target. Covering the full band requires two 48-MHz sub-arrays for the LBAs and three for the HBAs. Such broad and dense spectral coverage is crucial for our understanding of the intrinsic processes in pulsar magnetospheres and propagation effects through the interstellar medium at low radio frequencies (see Sect. 4).

Individual stations can also be used independently to conduct targeted observations of known bright objects, or wide field monitoring of transient events. In this respect, the international LOFAR stations have the highest sensitivity and may be available during normal LOFAR observations when the longest baselines are not in demand. In addition to the conventional mode where single stations are controlled through the central LOFAR facilities and send data back to CEP, the data will be recorded and analysed locally, so that each station can operate as a standalone instrument, or a group of stations could operate as a coordinated sub-array.

5.4. Polarisation

After careful calibration, LOFAR will enable polarisation studies of pulsar emission physics and the interstellar medium. A multi-stage process is required to achieve sufficient polarisation purity. We only summarise the most relevant issues here and refer the reader to the Magnetism Key Science project (Beck 2007) for more details. Both the LBAs and the HBAs have dual linearly polarised feeds that are stationary on the ground, meaning that for most observations the beams will be formed off-axis, potentially increasing the contribution from polarisation leakage. The dipoles are aligned South-East to North-West and South-West to North-East for the x- and y-dipoles respectively and this means that as a source is tracked across the sky the projected length of the dipole will change for the majority of sources. Thus, it will be important to accurately calibrate the gains of the individual dipoles. For all antennas and stations, Mueller and Jones matrices (Tinbergen 1996; Hamaker et al. 1996) need to be determined to correct for voltage and Stokes-parameter coupling. It is important to note that the beam patterns are time-variable and different for each station, however as discussed below it will be possible to calibrate the system in all but the worst ionospheric conditions.

To calibrate the individual LBA dipoles and the HBA tiles in a given station, delay lookup tables that provide static polarisation calibration will be used initially (see also Fig. 11). However, a multi-level calibration procedure based on the individual station elements and the stations themselves is required to ensure polarimetric fidelity as outlined in Wijnholds & van der Veen (2009, 2010b). Combining the stations to form tied-array beams when including stations beyond the superterp, will require using dynamic delays provided by the real-time calibration described above.

The LOFAR real-time calibration will correct for the ionospheric phase delays, but removing the ionospheric Faraday rotation is more challenging. The limited size of individual stations means that the ionosphere in most cases will not cause significant distortions across a station, ionospheric Faraday rotation introduces a differential, and frequency dependent, polarisation component in addition to the differential delays. If the properties of the ionosphere above each station are determined, the ionospheric Faraday rotation can be removed by applying a frequency dependent phase term to the complex polarisations at the level of each station. The polarisation data of the array can then finally be used to form 4 independent Stokes parameters, for both the incoherent sum mode as well as for the phased-array polarimetric observations, and subsequently processed as part of the pulsar pipeline using the methods described in van Straten (2004) and van Straten et al. (2010).

5.5. Transient buffer boards

The TBBs (see Singh et al. 2008) are an exciting and unique aspect of LOFAR. At each station there is sufficient memory, RAM, to store the full-bandwidth raw voltage data from all of the active elements in that station for up to 1.3 s[12]. These data can then be used to form an image anywhere in the visible sky, in the case of the LBAs, or anywhere in the element beam of the HBAs if a trigger, either external or internal, arrives within 1.3 s of an event occurring, and causes the data in the buffer to be frozen. This mode will be used predominantly by the Cosmic Ray Key Science Project (Falcke & LOFAR Cosmic Ray Key Science Project 2007) but will also be an invaluable tool for the Transients Key Science Project. It will be used to localise sources, but to also search for new transient events at very high time resolution.

The TBBs can also be operated in a mode where data are saved that has passed through the polyphase filter at the station. This allows one to choose a reduced bandwidth, B_r, and so significantly increase the amount of time which can be stored in the buffer: 1.3 s $\times$ 100 MHz/B_r. This mode will be very useful when expecting triggers related to short duration bursts at shorter wavelengths as the unknown dispersion delay in the interstellar medium may be many seconds.

6. LOFAR pulsar pipeline

In this section we describe the standard and automated "pipeline" processing that is applied to the LOFAR beamformed data produced by the various modes described in Sect. 5. We collectively refer to this processing as the "Pulsar Pipeline" though these data serve a broad range of scientific interests, not only pulsar science.

The processing is split into two major, consecutive segments: "online" processing, which is done by a Blue Gene P (BG/P) supercomputer to streaming data from the LOFAR stations, and "offline" processing which is further processing of these data on the LOFAR offline cluster (or potentially elsewhere). This hardware is located in Groningen in the Netherlands and the combination of the BG/P and offline cluster is known as CEP. The online processing is chiefly responsible for combining data from multiple stations into one or multiple beams[13], while the offline processing is more science-specific and includes, for example, dedispersion and folding of the data at a known pulsar period.

Given that the processing of the raw station data is done entirely in software, the pipeline is very flexible and extendable.

[12] This number may increase in the near future with the addition of more memory.

[13] As well as optionally producing correlations for imaging as described in Sect. 5.

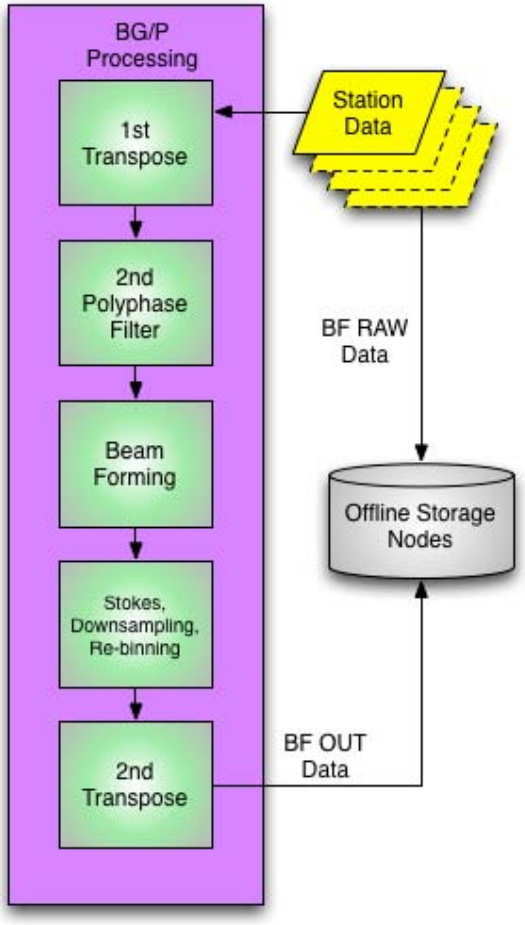

Fig. 5. Schematic diagram of the "online" Tied-Array Beam (TAB) Pipeline, as it runs on the BG/P. Streaming data from LOFAR stations are either written directly to disk per station ("BF RAW Data") or are read by the BG/P for pipeline processing in memory, combining station data into one or multiple beams, and then writing them to disk ("BF OUT Data").

Here we describe the current implementation and near future plans with the expectation that this will continue to evolve to meet new scientific requirements and to take advantage of increased computing resources in the future.

6.1. Online processing

Here we briefly describe the online processing chain as it applies to pulsar-like data. For reference, Fig. 5 shows a simple block diagram of the processing chain. For a more detailed and general description of the LOFAR correlator see Romein et al. (2010).

6.1.1. Station data

Each one of the LOFAR stations is capable of sending up to 244 subbands, that are either 156 or 195 kHz wide, to CEP in Groningen[14]. The subbands generated at the stations are sent as complex numbers representing the amplitude and phase, allowing division into smaller frequency channels if required, and the coherent or incoherent combination of stations. As discussed in Sect. 2 the subbands can be distributed over a non-contiguous range of frequencies and divided into station beams which can use different, or the same, set of subbands (see van Haarlem et al., in prep., for further details of station capabilities and data products). The station signals are fed to the BG/P, which can combine them into coherent and/or incoherent array beams, correlate them for imaging or in fact, produce all three data products at once.

The data flow is arranged so that each input/output (I/O) node of the BG/P handles all the data from one station, which is sent in 1 s sections we refer to as chunks. These 1 s chunks are then passed, in a round-robin fashion, to one of the 16 compute nodes attached to each of the I/O nodes (see Overview of the IBM Blue Gene/P Project (2008) for a description of the BG/P architecture). The compute nodes must finish the full online pipeline processing, and send the data back to the I/O node to be written out, before the next 1 second chunk of data arrives. There are sufficient computing resources that while keeping up with the real time processing there is approximately 16 s of available computing time for each 1 s chunk of raw data[15].

6.1.2. First transpose

The data arrive at the BG/P such that they are arranged by station, however in order to efficiently form correlation products and beams it is necessary to have the data from all the stations for a particular subband, in the 1 s chunks, present. The process of reordering these data is referred to as the "First Transpose" (Fig. 5). Before the transpose, the memory of a particular compute node holds multiple frequency subbands from a single station; after the transpose, the same compute node holds subband(s) of a particular frequency from all the stations being used.

6.1.3. Second polyphase filter

Depending on the particular application, each subband can be further split into an optional number of channels (16–256) via a polyphase filter (PPF). This is referred to as the "2nd polyphase filter" (2PPF, see Fig. 5), because of the preceding PPF step which occurs at the stations themselves in order to create subbands (see Sect. 2). This further channelization serves two purposes: it allows for the removal of narrow band interference signals in a way which minimises the loss of bandwidth; it is also required for incoherently dedispersing the pulsed signal. The removal of radio frequency interference (RFI) will be discussed in more detail below, but typically these signals are significantly narrower than the 156/195-kHz subbands sent from the stations, so further division into finer frequency channels is required (see Sect. 8 for details).

As discussed in Sect. 3, any broadband pulsed signal will be dispersed, and hence smeared in time, by the ISM between the source and the Earth. This can be corrected by either incoherent or coherent dedispersion. Coherent dedispersion will be used for studying known pulsars, as it provides the best possible dispersive correction along with the highest achievable time resolution for a given bandwidth. Since this technique is computationally very expensive, it is unfortunately not yet feasible to use coherent dedispersion for wide-area pulsar surveys, where it would need to be applied over large numbers of tied-array beams and trial DMs (thousands of trial DMs in the case of blind

[14] We do not consider here the details of the processing that happens at the stations themselves but refer the interested reader to de Vos et al. (2009).

[15] This is because there are 244 (i.e. approximately 256) subbands divided over 4096 available compute cores.

searches for millisecond pulsars). The survey processing chain will therefore operate on data which has been through the 2PPF and use computionally efficient incoherent dedispersion algorithms. Recently we have been able to develop a system which can perform coherent dedispersion for up to 40 different dispersion measures at one time (Mol & Romein 2011). This will have application as either a hybrid option where it is combined with incoherent dedispersion for large area surveys, or using coherent dedispersion for searches of objects where the DM is constrained to a limited range of values, such as in globular clusters.

6.1.4. Beamforming

It is at this stage that the (optional) beamforming between multiple stations is done (Fig. 5). The stations are combined in one or potentially several of the ways described in Sect. 5. This is performed on a per subband or even per channel basis depending on whether the data has been through the 2PPF. For incoherent beams, the combination is not done on the complex samples, but instead on the Stokes parameters (see also below). The geometrical delays between stations are computed once per second and interpolated both in frequency and time, so that each sample is corrected by a per-sample unique factor. The small number of possible incoherent beams, only one per station beam, means that this is not a computationally heavy task compared with the other calculations of the online processing; nor is the data rate unmanageable (see Table 3). Hence, incoherent array beams can, and often will, be produced in parallel to the correlation products needed for imaging or any other data-products, such as multiple tied-array beams.

In the case of tied-array beams, computational efficiency is a far greater concern, as up-to several hundred beams must be synthesized in parallel in order to give this mode sufficient "survey speed" for all-sky surveys. Beam forming is performed by applying the appropriate time and phase correction to the complex samples (Sect. 2). These delays are applied in three steps: first shifting by integer amounts of samples, then a phase correction for the center beam (these are both shared with the imaging pipeline), and finally a delta-phase correction between the center beam and each tied-array beam is applied. Determining the phase corrections due to contributions from the ionosphere and the instrument, which need to be calculated from the data, are discussed in Sect. 5. An efficient algorithm, partially written in assembly code, is used to maximize the number of beams that can be calculated. The large number of beams also make the data rate much larger, and the 15 Gb/s designed input limit of the current offline storage cluster plays the main limiting role on the maximum number of beams that can be written out. The final LOFAR offline cluster will have an increase in throughput of about 500%.

To form both incoherent and tied-array beams it is necessary to define a reference phase location. It is strongly preferable for observations where precise time tagging of events is required, such as pulsar timing, that this location be fixed. For LOFAR the phase center of all observations is now by convention the geographical center of the LBA field of station CS002, regardless of whether this particular station is being used or not. This places the official position of the LOFAR telescope at (x, y, z) coordinates of (3826577.462 m, 461022.624 m, 5064892.526 m) in the ETRS89 system (Boucher & Altamimi 2001). This reference position will be used for barycentering, pulsar timing, and phasing-up the array.

6.1.5. Fly's eye mode

For Fly's Eye mode, in which the station signals are *not* combined into incoherent or tied-array beams at BG/P, the processing proceeds largely as described above, except that individual station beams are written out separately using the same code that stores multiple tied-array beams. In parallel, it is also possible to generate the incoherent sum of the station beams if desired. Besides the scientific applications made possible by the huge FoV achievable with this mode, it is particularly handy for debugging issues related to individual station data because it allows for the comparison of ideally identical stations. Moreover it is useful for discovering sources of local RFI.

6.1.6. Stokes parameters, downsampling, and re-binning

Prior to beam forming, the individual time samples are in the form of two 32-bit complex numbers, representing the amplitude and phase of the X and Y polarisations of the antennas. From these, it is possible to calculate the 4 Stokes parameters, I, Q, U, and V online, assuming incoherent dedispersion is to be used, or to record the complex samples for offline coherent dedispersion. The 4 Stokes values fully encode the polarisation properties of the signal and can be used for polarimetric studies. Calibration of the polarisation products is discussed in Sect. 5.4.

To reduce the data rate one can optionally output only Stokes I, the total intensity. This is sufficient for many observations, and is preferable in the case of large-scale surveys where the data rate is already a major issue. Depending on the required sampling rate, the data may be downsampled in time and also scaled to re-pack the 32-bit Stokes parameters into 16-bit samples (this currently happens offline but will later be implemented on the streaming data). Application of RFI mitigation strategies to these streaming data may allow us to further reduce the data to 8-bit samples or less, which will reduce the data rate and hence potentially allow the formation of more tied-array beams.

6.1.7. Second transpose

At this stage, the necessary online processing is complete but the data products are spread across the compute nodes of BG/P in an order that is contrary to the way they are typically, and most efficiently, analyzed in further time-domain based scientific post-processing. Each of the compute nodes contains all of the synthesized beams, but only for a limited number of subbands. For dedispersion and other applications the data are best organized such that all the frequency channels of a particular beam are in one place. Thus a "Second Transpose" (Fig. 5) is carried out to reorganize the data across the various I/O nodes of BG/P before it is written to files on the offline cluster. This Second Transpose is critical for handling large numbers of beams in the offline processing. An added advantage of the Second Transpose is that it will also make it possible to recombine the subbands using an inverse PPF in order to obtain a time resolution close to the original ~10 ns resolution available before the subbanding of the data at station level. This mode may be of interest for detailed studies of giant pulses and for detecting the short radio flashes created by cosmic rays entering the atmosphere (Falcke & LOFAR Cosmic Ray Key Science Project 2007).

6.2. Radio frequency interference excision

The low-frequency window, 10–240 MHz, observed by LOFAR contains a range of interfering sources of radio emission: from

commercial radio stations, to weather satellites, to air traffic control communication. To mitigate the influence of this RFI on our data we have implemented some basic strategies, which we discuss below. We will not discuss the online RFI mitigation strategies employed by LOFAR as these will be discussed in detail elsewhere.

Our principal mechanism for excising RFI is to simply not observe where it is present. The FM-radio band from about 90–110 MHz is already filtered out within the LOFAR design (van Haarlem et al., in prep.). The station-based frequency channelisation of LOFAR to subbands of either 156 or 195 kHz, combined with the ability to spread these subbands anywhere within the available 80 or 100 MHz Nyquist zones, already provides the means to avoid commonly affected frequencies without sacrificing observing bandwidth. As will be shown below (Sect. 7.1.1) many of the interfering sources have bandwidths that are significantly narrower than the station-based subband width and so by performing the 2PPF step (Sect. 6.1.3) to increase the frequency resolution we are further able to excise RFI with a low impact on the total remaining bandwidth. Moreover, the majority of the interfering sources have a relatively low duty cycle and so only small sections of time may need to be excised in order to remove the interference.

Our present strategy to identify RFI in our data is such that for every frequency channel we calculate the quasi-instantaneous root-mean-square deviation (rms) of data chunks of duration ∼10 s. The rms calculation is performed after iterating to remove any bright data points which are likely to be RFI and biasing the determination of the rms. If a particular time sample is larger than 6σ above the rms then it is considered to be RFI. If there are more than 30% of such samples in the time series, then the whole frequency channel is marked as RFI-corrupted and will be excluded from further analysis. This RFI excision can be run both in manual mode and as part of our automated pipeline. In the automated mode we exclude only the corrupted channels, but leave the strong $>6\sigma$ individual samples if their fraction is less than 30%. We do this to avoid removing any very bright single pulses. This is not problematic since some short duration sparse RFI in the data will not dramatically impact the data quality. This is because the dispersion smearing, even for quite low DM values, is significant at such low observing frequencies. Thus, during the dedispersion process, the RFI, which is at a dispersion measure of zero as it has not propagated through the ISM, will be dispersed and thus contribute only extra noise and will not significantly distort the pulse profile (see Fig. 18 for an example).

6.2.1. Final raw data products

The raw data streaming out of BG/P, in some cases at the eventual rate of several GB/s, are written to multiple storage nodes of a large offline storage and processing cluster[16]. The data are currently written as almost header-less raw binary files, but will soon be stored using an implementation of the Hierarchical Data Format 5 (HDF5)[17]. The HDF5 file format was chosen because of its flexibility and its ability to store very large, complex datasets spread over many separate physical devices.

An overview of the beamformed file structure is shown in Fig. 6; it is too complex to describe here in detail (Alexov et al. 2010a,b). The hierarchical tree divides the data into the separate station beams, tied-array beams and the 4 Stokes parameters (shown) or the *X* & *Y* polarisation amplitude and phase values if complex data is recorded. For each beam and polarisation parameter, the signal as a function of time sample and frequency channel is stored in an array. Metadata fully describing the observation is stored both at the root level and along the tree where applicable. For instance, the parameters describing individual stations or tied-array beams are stored at the same tree level as these data themselves. Data processing and logging information are stored in the output beamformed HDF5 files in processing history groups; more general information is stored at the root of the file, while more specific information which pertains only to individual stations or beams is stored along the tree where applicable. Each beam has a coordinates group which describes the pointing information for that observation; the coordinates are analogous to the World Coordinate System (WCS) in the FITS format definition (Alexov et al. 2010a,b).

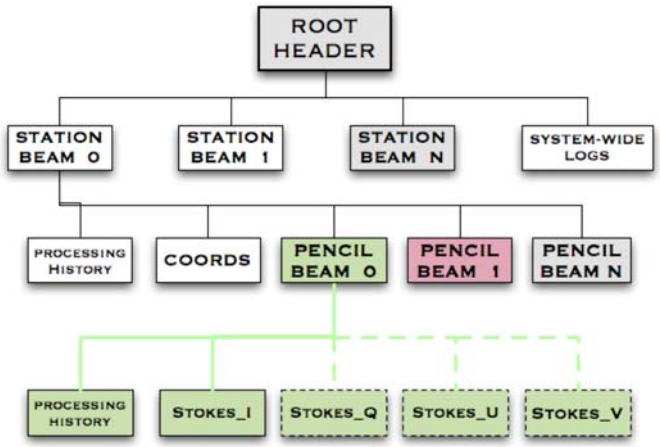

Fig. 6. An overview of the beamformed file structure, encapsulated in a hierarchical tree within an HDF5 file. The data are split into separated sub-array pointing (known in this paper as station beams); within each sub-array pointing are pencil or tied-array Beams (we will use tied-array beams), along with coordinates and processing information; each Beam contains a data structure with either 4 Stokes parameters (or just Stokes *I* for total intensity) *or*, if desired, the amplitude and phase of the *X* and *Y* polarisations separately. Header keywords are stored within each tree level, depending on their hierarchical relevance to the rest of the file, as the information is inherited as one steps downward through the tree structure. See Alexov et al. (2010a,b) for more details.

Though it is expected that LOFAR pulsar data will be archived in this format, we note that we have already written a flexible data converter in order to also write the data into several other community standard formats like the PRESTO/SIGPROC "filterbank" format and the PSRFITS format.

6.3. Offline processing

In Fig. 7 we show a block diagram of an example pipeline, in this case the "Known Pulsar Pipeline", describing the essential steps in the process. Similar pipelines are being developed for all the different processing streams as will be described below.

The raw data from the stations can either be written directly to the offline storage nodes, which is useful for sub-arraying or single station experiments, or they can be passed through the BG/P for further channelization, beamforming, and other processing. The starting point for all the pipelines discussed here is the beamformed data coming out of BG/P, be that incoherent or coherent beams (though see Sect. 6.5.1). It is possible to take

[16] http://www.lofar.org/wiki/doku.php?id=public:lofar_cluster#short_lofar_cluster_layout
[17] HDF home page: http://www.hdfgroup.org/

other data products, such as imaging visibilities or data dumps from the transient buffer boards, in parallel, but the processing of those will be discussed elsewhere.

6.3.1. LOFAR offline cluster

The offline processing pipelines run on the LOFAR Offline Cluster (LOC), which is the second main part of CEP. The data writing from the BG/P is distributed across multiple storage nodes on the LOC, the number of which can be chosen to match the data rate. The storage and compute nodes are grouped into sub-clusters, each of which contains 3 storage and 9 compute nodes. The 9 compute nodes of each sub-cluster can access the data on the 3 storage nodes via NFS. The current LOC comprises 8 such sub-clusters; this will soon be expanded as LOFAR approaches full capability.

After the data are written to the LOC it can either be passed directly to the long term archive if that is appropriate, though that will not normally be done due to the large volumes of the raw datasets. More usually the data will pass to one of the pipelines where data processing and compression happen.

6.3.2. Pipeline framework

All the LOFAR processing pipelines are built to run within a generic pipeline framework[18]. This framework takes care of distributing the processing in parallel over the LOC compute nodes, and provides appropriate logging and error checking. In the production system, the Pulsar Pipeline will start processing automatically either during or after an observation, depending on the data rate and availability of processing resources. The allocation of computing and storage resources, and observing time, will be handled by software referred to as the LOFAR Scheduler so that commensal data-taking and processing do not collide. The Scheduler will also be responsible for passing observation-specific metadata to the HDF5 header. Further header information will flow from the observing control systems SAS (Specification, Administration and Scheduling) and MAC (Monitoring and Control) into the HDF5 file as well via the *parset* (parameter set) as shown in Fig. 7.

6.3.3. Software and data access

Wherever possible, all of the different Pulsar Pipelines are being built around the well-tested, commonly used, open source software packages available in the pulsar community (e.g. PRESTO[19], PSRCHIVE[20], SIGPROC[21], TEMPO[22]. To allow for efficient development and software management these have been incorporated into the general LOFAR User Software (LUS)[23], which uses cmake[24], a cross-platform, open-source build system, to automate the installation of these packages on a variety of platforms (e.g. Ubuntu Linux and Mac OS 10.5.X). This cmake installer may be of interest to others using these same reduction packages on other systems.

The LOFAR software interface to the HDF5 library is called the Data Access Library (DAL). It is also available within the LUS software repository. The DAL allows for high-level connectivity to HDF5 data, and more specifically to LOFAR data structures encapsulated within an HDF5 file. The DAL is written in C++; it contains classes which pertain to all the LOFAR-specific data structures, making it straight forward to read and write LOFAR HDF5 data. The DAL is also bound as a Python module, called pydal, giving users access to the DAL classes via Python. This is an important set of tools for connecting existing or newly written processing code to the data.

6.3.4. Radio frequency interference excision

The Known Pulsar Pipeline in Fig. 7 shows two parallel processing paths in the offline reduction of LOFAR BF data. The standard path performs dedispersion and folding; optionally, the pipeline can be run on the same data, but having performed RFI-excision prior to folding and dedispersion. This process filters the data of RFI and then runs the same tools as run for standard processing. The data processing time doubles since the pipeline is essentially performing the same processing twice, once on unfiltered data and a second time on RFI-cleaned files. Once the RFI-cleaning algorithms have been refined, we expect to only run the processing once, using the RFI-cleaned data.

6.4. Known pulsar pipeline

The Known Pulsar Pipeline processes data taken in the following modes: Incoherent Stokes, Coherent Stokes, Coherent Complex, Fly's Eye and Commensal Imaging. In all cases, once the data is on the LOC, the processing done by the Known Pulsar Pipeline is very similar to standard pulsar processing (e.g. Lorimer & Kramer 2005). Once the data have undergone RFI excision it is then dedispersed at the known DM using either coherent or incoherent dedispersion, depending on the particular source and the scientific goals. The dispersion-corrected data will then be used to generate a number of output data products such as dedispersed time series, dynamic spectra and folded pulse profiles. It is likely that we will simultaneously observe multiple pulsars, and so multiple instances of the pipeline, with different dispersion and fold parameters, will run in parallel. The processing capability of LOFAR is such that we are in general able to produce all of these data products for each known pulsar observation. These data products are then flux and polarisation calibrated, stored to the long term archive as well as being passed to post processing programs. Multiple pipelines, from multiple separate observations, can run in parallel depending on the available computing resources on the LOC.

As well as these scientific data products the pipeline (Fig. 7) will also produce a series of "pulsar diagnostic plots" e.g. signal statistics, bandpasses, RFI occupancy and calibration information, which can be used to both calibrate the data and assess their quality. These will be stored in the long term archive. In some cases raw data products with lower time and frequency resolution will also be archived to allow further processing if needed. This will be particularly valuable when wide FoV modes are being used, as new sources might later be found in these same observations.

6.5. Periodicity and single pulse search pipeline

As described in Sect. 4, pulsar/fast-transient search observations are a key aspect of the LOFAR pulsar science case. These can be divided into at least five types of searches, each with its

[18] http://usg.lofar.org/documentation/pipeline/
[19] http://www.cv.nrao.edu/~sransom/presto/
[20] http://sourceforge.net/projects/psrchive/
[21] http://sigproc.sourceforge.net/
[22] http://www.atnf.csiro.au/research/pulsar/tempo/
[23] http://usg.lofar.org
[24] http://www.cmake.org/

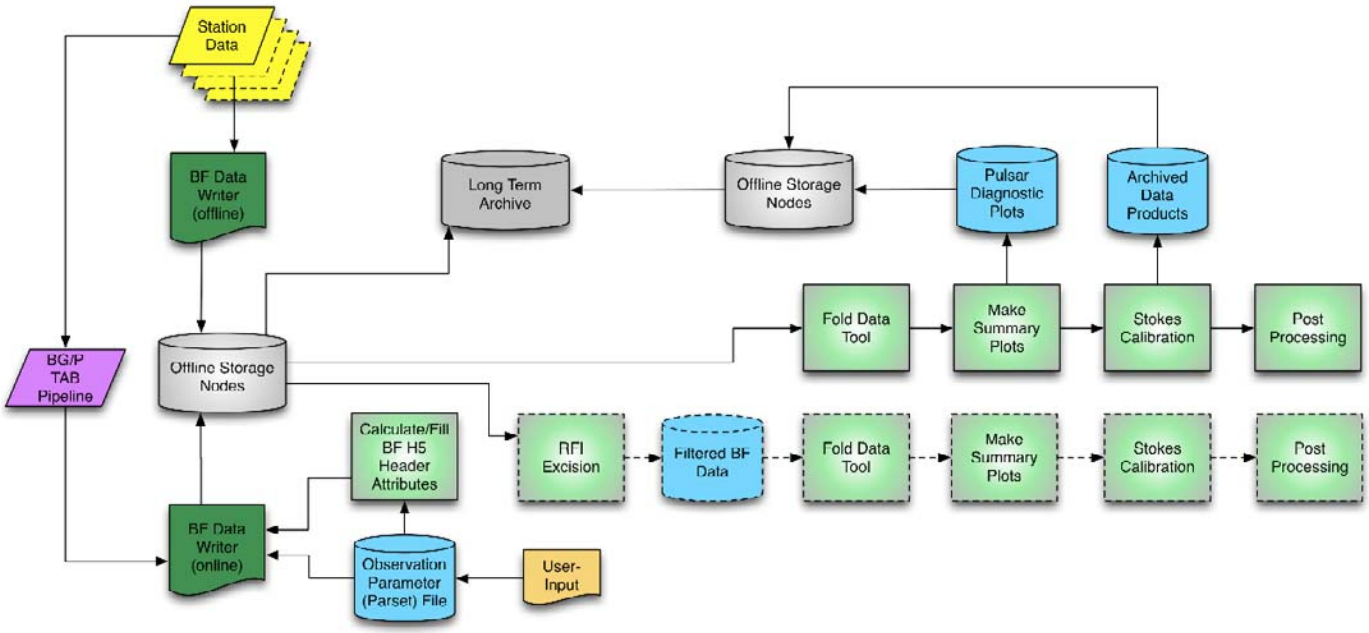

Fig. 7. Schematic diagram of the overall Known Pulsar Pipeline, as it runs "online" on the BG/P followed by "offline" scientific processing on the offline cluster. Offline pipeline processing can be run on data directly out of the BG/P or on RFI-filtered data. Scientific tools such as de-dispersion and folding are performed, along with Stokes calibration to get polarisation and flux densities. Data products and diagnostic plots are stored in the long term archive.

own corresponding data-reduction strategy and science goals. Together, these complementary approaches span a huge range of source parameter space (e.g., source brightness, recurrence rate of transients, and sky location):

- i) targeted searches of multi-wavelength sources using one or a few tied-array beams. Here maximum sensitivity is required over a relatively small FoV;
- ii) all-sky survey using hundreds of tied-array beams. This is the best option for a high-instantaneous-sensitivity all-sky pulsar/fast-transient survey. However, the small FoV of tied-array beams will limit the possible dwell time to roughly 10 min;
- iii) all-sky survey using (multiple) incoherent beams. This provides a shallower survey in terms of raw sensitivity, but the large FoV of potentially multiple incoherent beams makes 1 h (or longer) dwell times feasible;
- iv) wide-area Fly's Eye searches for rare, bright transients. Pointing the station beams in different directions allows even longer dwell times, with reduced sensitivity;
- v) Piggy-back observations using a single incoherent beam. These intend to maximize the product of total on-sky observing time and FoV in order to detect the rarest transient events. Ultimately, this could provide on the order of a full day's worth of integration time over the *entire* LOFAR-visible sky on the timescale of a few years.

6.5.1. General search requirements and processing

We currently have a basic search pipeline in place that can deal well with searching a single incoherent beam or a few tied-array beams. However, modes using hundreds of tied-array beams require highly optimised processing chains and the full LOC hardware to be in place, and so we are currently only in the planning phase of this more complex mode[25]. As well as potentially dealing with large numbers of beams, the very low frequencies and wide fractional bandwidths involved in the pulsar searches means that in the Pulsar Search Pipeline, the number of trial DMs will be at least 10 000, which clearly makes dedispersion one of the rate limiting steps. We are therefore in the process of designing an optimal mechanism to efficiently process pulsar search data within the CEP framework. As well as considering hybrid coherent/incoherent dedispersion modes we are looking at moving some survey processing on to the BG/P. Distributing and parallelizing the pipeline will be done by the Pipeline Framework; however, the mechanism itself of how data processing will be performed and which algorithms will be used on the LOC are still being determined.

We now consider the different envisioned search modes in more detail:

Targeted searches. Targeted searches of known, multi-wavelength sources require maximum sensitivity over a relatively small area of sky compared with the ~20 sq. deg single station beam FoV. This mode will therefore use a number of tied-array beams, the total required number depending on the size of the source or its positional uncertainty. If the number of beams is significantly less than needed for the all-sky survey, then the load on BG/P and the offline cluster will be modest and so simultaneous imaging modes are likely to be run in parallel. For this, and other modes which use tied-array beams, one beam may be sacrificed to point well away from the target area and be used as a reference beam for RFI excision. Potential targets for such searches include, e.g., unidentified Fermi γ-ray sources, apparently radio quiet γ-ray/X-ray pulsars, magnetars, and nearby galaxies or globular clusters.

[25] Note that this processing challenge is still only a fraction of what will be required for the SKA.

All-sky coherent (tied-array) survey. The planned all-sky tied-array survey will be by far the most data and computation intensive implementation of the pulsar pipelines. The optimal way to perform the survey is with, at least, a couple of hundred tied-array beams. A maximal implementation will result in a data rate of order 23 TB h^{-1}. We are currently pursuing two options for the survey processing, which depend greatly on the mix of computing resources and storage capacity. If the latter is the most restrictive then a real-time processing chain may be needed, where dedispersion, FFT'ing, and candidate selection will be done in close to real time with only data products related to the resultant candidates being stored. Alternatively, relatively short observing sessions will take place with data being stored and processed at a later date. The latter approach is preferable, but some hybrid process may be required. Such a survey provides the highest possible raw sensitivity, but the dwell time per pointing will have to be modest because of the limited FoV. Certain classes of intermittent sources may be better sampled by an all-sky survey using incoherent beams (see below).

All-sky incoherent survey. The raw sensitivity of incoherent array beams (using say all 40 Dutch stations) is roughly 3 times lower than the sensitivity of tied-array beams made from the combination of all 24 core stations. Nonetheless, these incoherent beams have over 1000 times larger FoVs, making shallow all-sky surveys in this mode an attractive possibility because of the ability to use long dwell times. Using multiple station beams, the FoV can be increased even further. For instance, using 7 station beams provides an instantaneous FoV of ~170 sq. deg, at a central frequency of about 140 MHz, allowing one to search the entire LOFAR-visible sky ($\delta > -35°$) with only 200 pointings. Even with a 1 h dwell time, such a survey can be completed in roughly 1 week of observing time. Shallow surveys such as the example described above are not only much more tractable in terms of required observing and processing time, but they also provide an excellent complement to deep all-sky surveys with higher instantaneous sensitivity. This is because some intermittent sources, e.g. the RRATs, may be easier to identify in surveys where the product of FoV and dwell time is large (assuming the underlying sensitivity is also sufficient).

Fly's Eye searches. Very bright but rare transients may be better found by surveys that sacrifice even more raw sensitivity in favor of increased FoV and dwell time. Fly's Eye searches will be processed in a similar way to the all-sky surveys, except that different data streams will correspond to individual station beams pointing in a variety of directions, instead of different tied-array or incoherent array beams. There could be up to a couple hundred such beams depending on how the observing bandwidth is distributed among individual station beams. This provides, in principle, the ability to monitor the *entire* LOFAR-visible sky at once making LOFAR a truly synoptic radio telescope.

Piggy-back searches. Piggy-back searches aim to achieve the maximum possible on-sky time for transients by observing in parallel whenever possible. This mode will be run as often as possible when the telescope is doing standard imaging observations or even during tied-array observations. It will use only one incoherent or a few tied-array beams and so the computational load is reasonable. The simultaneous imaging data might be used when interesting candidates are found. These relatively shallow, but typically wide FoV observations allow for repeated studies of the same piece of sky in order to probe variable and transient sources. The additional processing requirement is small compared with that required for imaging.

Single station processing. In Single Station mode, the network streams carrying the data that would otherwise go to the BG/P need to be redirected to local servers. This involves for the most part the 48 MHz of beamformed data, which are streamed through 4 UDP[26] streams of approximately 800 Mb s^{-1} each. Members of the LOFAR pulsar collaboration have developed a hardware and software solution (codenamed ARTEMIS) acting as a single station backend and capable of recording data for observations of pulsars and fast transients. This backend has the processing power required to perform a number of relevant operations in real time, such as RFI excision, channelisation, and Stokes parameter generation. It is also designed to connect to fast Graphics Processing Units for real time dispersion measure searching on the streaming data. Besides pulsars and fast transients ARTEMIS can be used as a general purpose single station backend. Such an instrument allows observations to be made either in parallel with ongoing central LOFAR observations, or allow for local processing when the station is in local or remote control if there are insufficient BG/P resources for the required processing. Moreover it allows for the possibility of processing and analysing larger data sets than can be transferred to the Netherlands.

7. Commissioning results

Since pulsar "first light" in the summer of 2007, when there were only a few test antennas available, we have been commissioning the LOFAR telescope for pulsar observations. In this time, LOFAR's sensitivity and functionality have increased dramatically, as has the data quality (for the progression, see Stappers et al. 2007; Hessels et al. 2009, 2010; Stappers et al. 2011). The ability to detect bright pulsars with just one or a few individual HBA tiles means that pulsar observations are useful for measuring the system performance from some of its smallest elements up to the full, combined array. For instance, pulsar observations can be used to study the beam shapes of individual or beamformed elements, verify antenna positions, and measure clock stability. Here we present highlights from some of these system tests, followed by associated early science results. These demonstrate that LOFAR is beginning to function as designed.

Though already impressive, these observational results provide merely a taste of what LOFAR will ultimately be capable of doing. The number of completed stations is still increasing and we have only just begun to take data with coherently combined stations. Also, proper phase calibration of the LOFAR stations is currently being implemented and will increase the raw sensitivity by up to a factor of 2–3 (Fig. 11). Therefore, we expect that many of the observations presented here will be surpassed in the coming year(s) by increasingly sensitive measurements using the full breadth of LOFAR.

7.1. Observational tests of the system

7.1.1. Radio frequency interference

In order to monitor the LOFAR RFI environment, we have recorded which frequency channels are badly corrupted in each

[26] User Datagram Protocol.

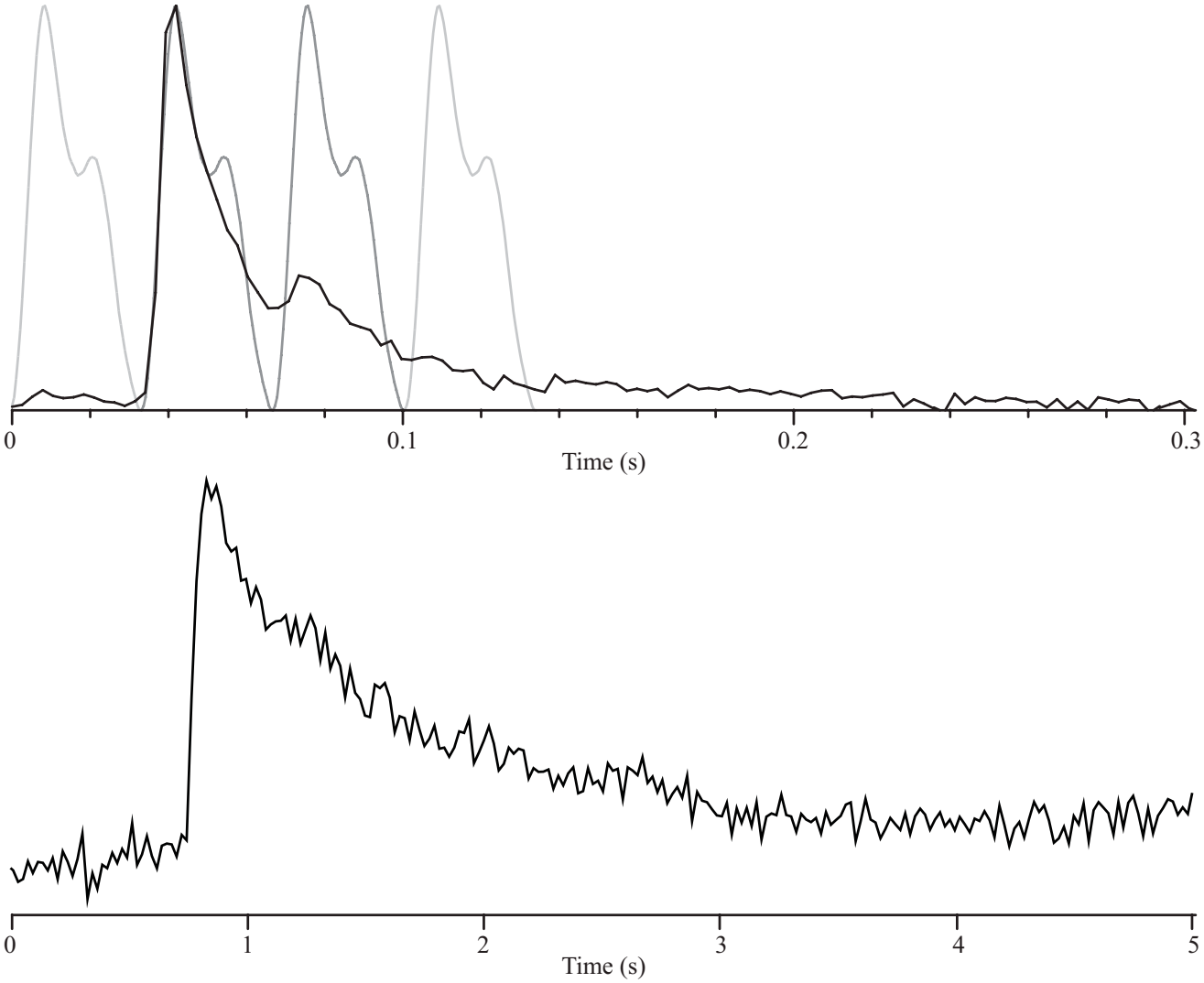

Fig. 8. Observations of giant pulses from PSR B0531+21 in the Crab Nebula observed with both the HBA and LBA. The *top panel* shows a "double giant" pulse observed using the incoherent sum of the HBAs from 6 core stations over the frequency range 139–187 MHz. A section of the timeseries data (black line) is shown indicating a giant pulse which is followed by a second giant pulse in the next rotation of the pulsar. The fading grey lines show the average pulse profile for this observation repeated four times. The two giant pulses clearly show the influence of scattering in the ISM and from the Crab Nebula itself. The *lower panel* shows a single giant pulse observed with the LBAs from 17 core stations added incoherently over the range 32–80 MHz. Note the significantly different timescale for the scattering delay compared with the HBA observation.

given observing session. Collating the statistics from many observations, we are able to determine which specific channels are more consistently contaminated by RFI than others. With this information we can then carefully select which channels to avoid when choosing the channels to process. If whole subbands are seen to be dominated by RFI we can also not select those when transferring data from the stations. Figure 9 shows the histograms of corrupted channels as a percentile of the total number of observations that included that particular channel. These data do not show the full LOFAR observing range, as they reflect the frequency range most commonly observed in these commissioning observations (which was chosen to optimize sensitivity for pulsar observations).

We have used more than 350 observations in the HBAs and more than 50 bservations with the LBAs, spread over about a 3 month period and occurring during both day and night-time. We compare the statistics for subbands, the 195 kHz channels delivered directly by the stations, with those of the typically 12 kHz channels created by the second polyphase filter on BG/P. One can see that in the majority of frequency channels the fraction of observations affected by RFI is less than a few percent, with a higher total percentage of the band being affected at the low end of the LBA range. It is also noticeable that in the majority of cases the RFI is unresolved in the broader 195-kHz subbands, meaning that by further channelising the data we lose a smaller percentage of the available band[27]. These results are extremely encouraging and indicate that in general, RFI, if they stay at these levels, will have a limited detrimental effect on pulsar observations.

7.1.2. HBA sub-station beam shape comparison

The two 24-tile HBA sub-stations associated with each core station can be used separately or combined coherently at station

[27] Tests from imaging observations indicate that a good fraction of the narrow-band RFI is only resolved at the 1-kHz level.

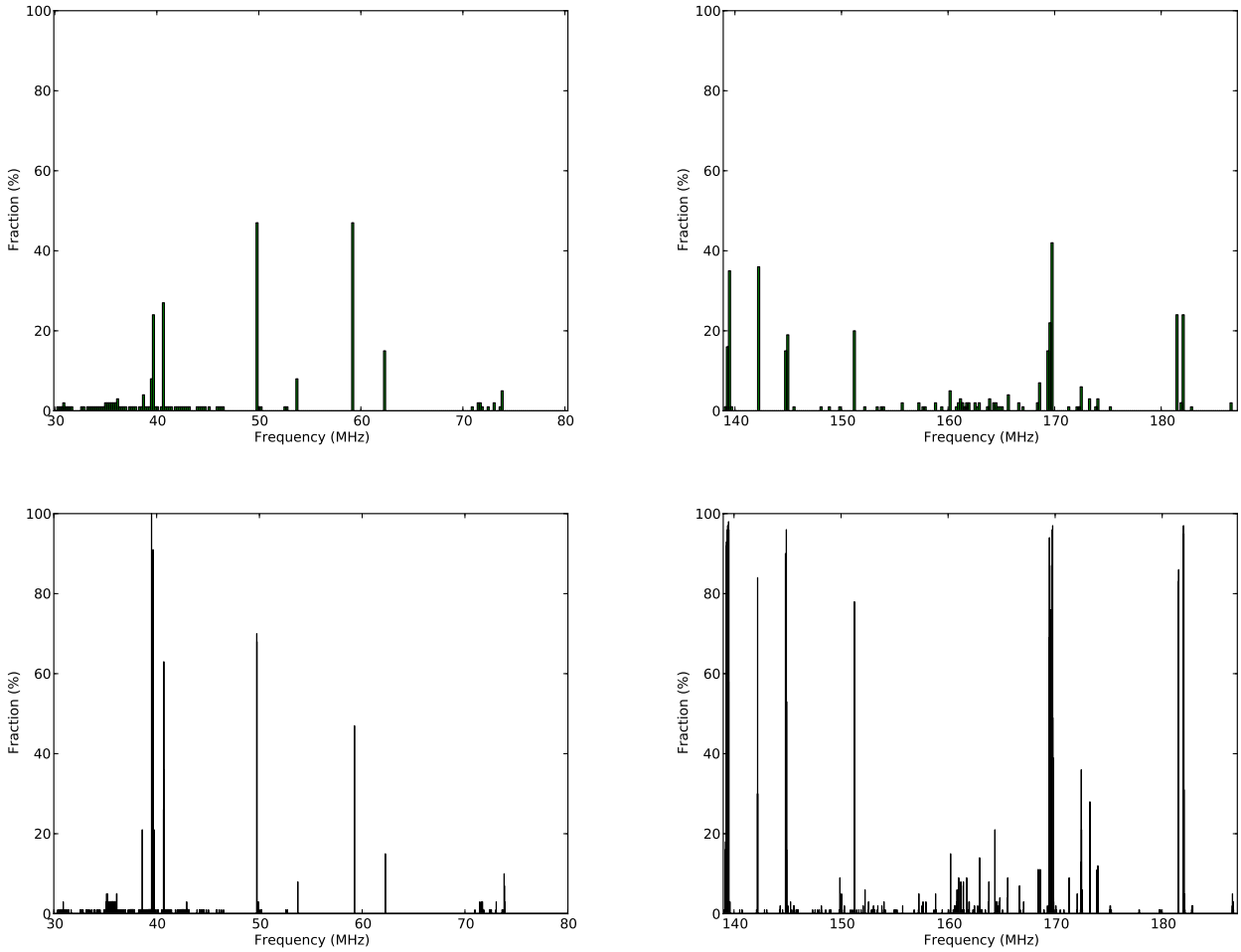

Fig. 9. An initial summary of the RFI situation across our most commonly used sections of the LBA (*left-hand panels*) and HBA (*right-hand panels*) frequency ranges. The upper and lower panels correspond to a frequency channel width of 195 kHz and 12 kHz, respectively. Each line in the plot corresponds to the percentage of observations in which the particular frequency channel was affected by RFI.

level. In order to verify that a truly coherent addition of the two sub-stations was taking place, and to confirm that the resulting beam shape agreed with theoretical expectations, we performed an experiment in which the two sub-stations were pointed at the Zenith and did not track a celestial position. Data were then recorded as the very bright pulsar B0329+54 transited through the beam[28]. The resulting "fringe" pattern is shown in Fig. 10. As the pulsar enters the single-sub-station beam, it becomes visible and the detected intensity then varies as a function of time as the pulsar passes through the fan-beam pattern that results from the coherent addition of the two sub-stations. A simple comparison of the time between maxima, 500 s, agrees with what is expected for two sub-stations separated by 120 m, at a central observing frequency of 165 MHz. This conclusively verifies that the sub-stations are indeed being added coherently.

7.1.3. LBA station calibration

Beam-server software has been implemented in order to apply static calibration tables that correct for the remaining phase differences between the individual elements at each of the stations (e.g. uncorrected differences in cable lengths). This is necessary in order to make a true coherent addition of the station antennas, which maximizes station sensitivity and produces a cleaner station beam shape. These calibration tables are calculated empirically from 24 h calibration runs, whose long length aims to reduce the influence of ionospheric turbulence and RFI present in individual observations. These long term values will only need to be updated infrequently and will be augmented with a few minutes of observations on bright calibration sources. As can be seen in Fig. 11, station calibration of the LBA antennas is now in place and is providing a sizable increase in raw sensitivity. This is particularly important as LBA pulsar observations are strongly sensitivity limited. We note that station calibration for the HBAs has also recently been implemented.

7.1.4. Simultaneous imaging and pulsar observations

As discussed earlier, the ability to simultaneously image the sky *and* record high-time-resolution, beamformed data increases the observing efficiency of the telescope and affords new scientific opportunities. We have performed a number of simultaneous imaging and pulsar observations to test the functionality of this mode. Shown in Fig. 12 is a 12 h observation of a field including

[28] The latitude of the core of LOFAR is 52.°9 and the 5.°5 single-sub-station beam is wide enough to encompass the transit of this source.

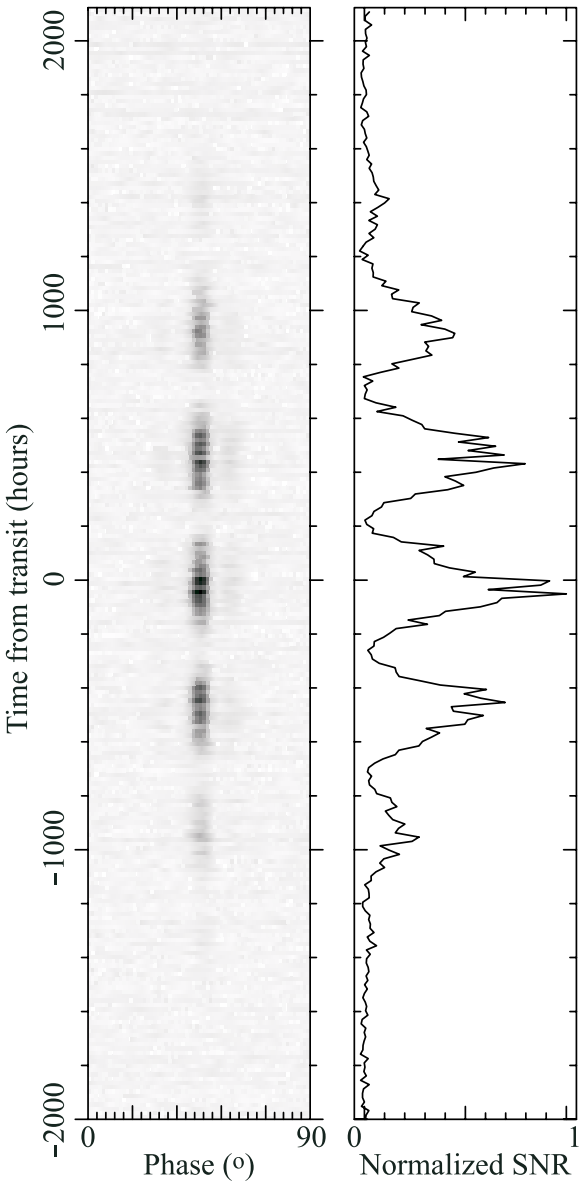

Fig. 10. A transit observation at a central frequency of 165 MHz of PSR B0329+54 as it passes through the zenith above core station CS302. The antennas were combined coherently without further geometrical delay in order to point directly above. *Left*: the intensity of PSR B0329+54 as a function of time from transit and rotational phase. The variations are due to both the "fringe" pattern created by the coherent addition of the two HBA sub-stations of station CS302 and the wider single sub-station beam width. *Right*: the corresponding normalized S/N of the pulsar as a function of time from transit.

the bright pulsar B0329+54 (with a flux density at 100 MHz of $S_{100} \sim 1$ Jy). These data were taken on 2010 April 19 and included 7 core and 3 remote stations. An initial calibration was made using the three brightest sources in the field, the brightest of which was placed at the phase center. These observations have an odd point spread function (PSF), which is the result of there being only short and long baselines, with little uv-coverage on intermediate baselines. Note however that the image here has been "cleaned", largely removing this effect. Current observations are already using significantly more stations and far better (u, v)-coverage.

7.1.5. Multiple station beams

To demonstrate the ability of LOFAR stations to create multiple beams on the sky (at the expense of total bandwidth per beam), we performed an observation in which two station beams, of ~24 MHz bandwidth, each simultaneously tracked the pulsars B0329+54 and B0450+55 for 0.5 h. The system was configured such that the ~20°-wide element beam of the HBA tiles was pointed half-way between the two pulsars, which are separated by about 12° on the sky. The resulting pulse profiles can be seen in Fig. 4 and an illustrative graphic can be seen in Hessels et al. (2010). It is worth noting that this angular separation is far larger than what is possible to observe with a multi-beam receiver or a focal plane array. Though the HBA system, using the full sensitivity, is limited to creating multiple station beams within the 20°-wide tile beams, the LBA dipoles do not have this extra level of beamforming and each has a roughly 120°-wide beam, making it possible to simultaneously observe sources *almost anywhere* above the local horizon. In fact, such observations have recently been made in which 6 pulsars distributed across the intantaneous LBA FoV were simultaneously observed.

7.1.6. Observing with multiple stations

As demonstrated below, individual LOFAR stations are sensitive telescopes in their own right. Combining the 24 stations in the LOFAR core will increase sensitivity over that of a single station by up to a factor of about 5 or 24 depending on whether the addition is incoherent or coherent respectively (see Sect. 2). We have performed a series of observations comparing the measured S/N of the pulsar B1508+55 for different numbers of stations added. The increase in S/N seen in these profiles agrees well with the theoretical expectation that the S/N should increase with the square-root of the number of stations which have been incoherently combined (see Hessels et al. 2010). We will continue to test this relation as more LOFAR stations come online, especially to verify that coherently added stations are delivering the expected sensitivity increase (see below). It is possible that RFI local to individual stations will also affect the summed signal, although less dramatically if they are more distant and we are forming the coherent sum, and so we are exploring options to flag these stations online and dynamically remove them from the combined beam.

7.1.7. Early (Superterp) tied-array observations

With the installation of a system to provide a single clock signal to all of the stations located on the Superterp (6 LBA core fields and 12 HBA sub-stations), the task of calibrating tied-array beams between these stations was greatly simplified. By observing a bright calibrator source in imaging mode, it is possible to solve for the phase offsets between stations and then apply these corrections to future observations. Experience shows that the phase offsets between Superterp stations, which should most of the time see the same ionospheric patch, for the majority of the frequencies we are considering here are sufficiently constant on timescales of hours to ensure that the gain in the direction of the pulsar remains optimal. Our commissioning observations so far have shown that coherent addition produces an improvement in the S/N compared with the incoherent sum by a factor of $\sqrt{n_{\rm stations}} = \sqrt{12} = 3.5$ as would be expected for tied-array addition to be working (see Fig. 14).

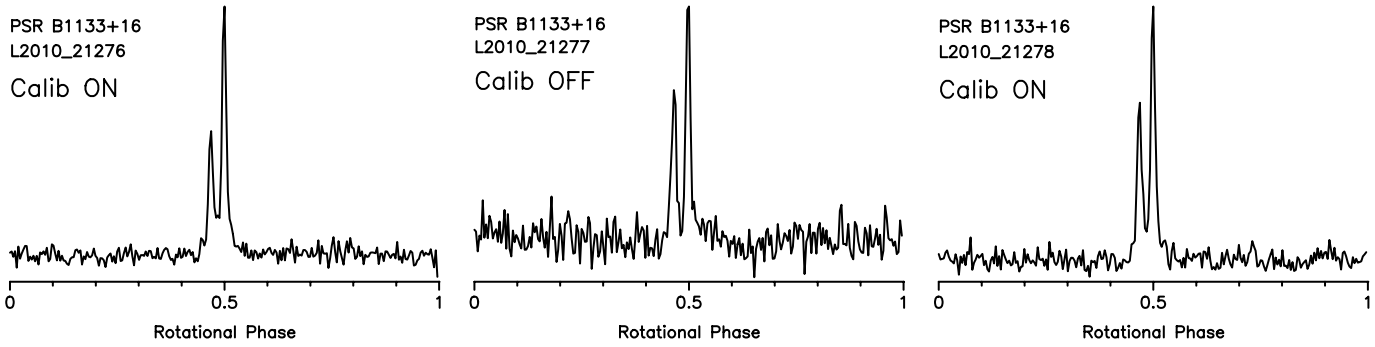

Fig. 11. Three consecutive 20 min LBA observations of PSR B1133+16 taken on 2010 Nov. 5. In between these observations, the station calibration was alternately turned off and then back on. The profiles are all scaled to have the same peak height and as can be seen, the S/N of the cumulative pulse profile decreases by roughly a factor of 3 when the static calibration table is not applied. Five Dutch stations were combined incoherently in these observations, and as such the S/N difference is the average calibration gain for all these stations.

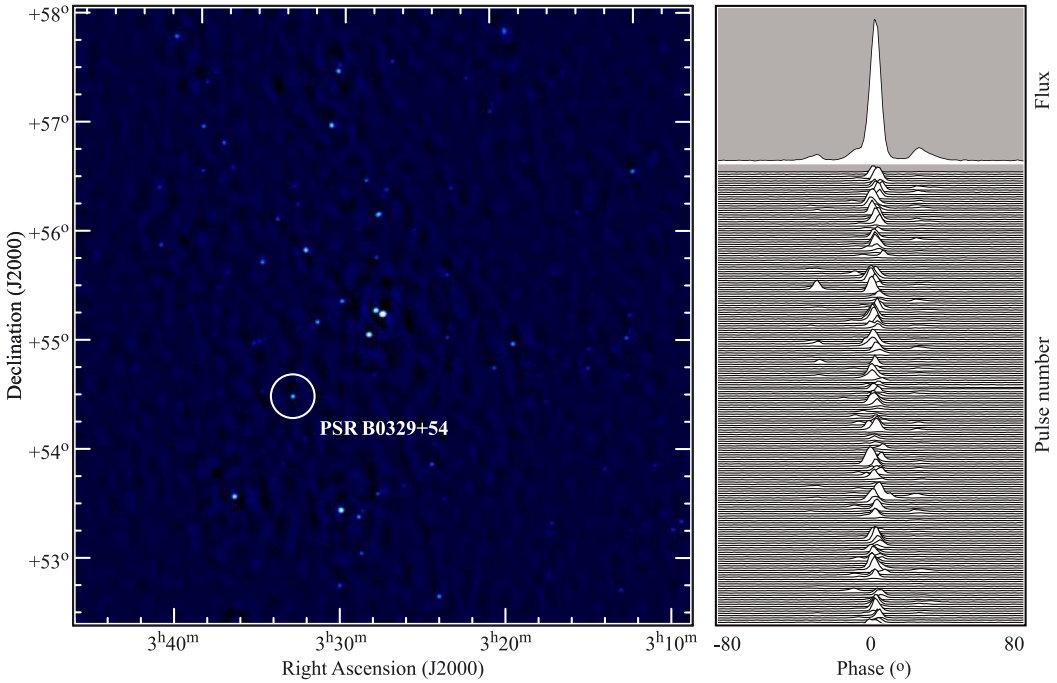

Fig. 12. *Left*: LOFAR HBA image (139–187 MHz) of a 5.°5 × 5.°5 field including PSR B0329+54, which is circled. The phase center of the image was pointed to the brightest nearby source, the 40 Jy: 3C 86. The dynamic range in the image is about 1600 and the resolution about 100″. *Right*: pulse stack of roughly 200 individual pulses from PSR B0329+54, detected in simultaneously acquired beamformed data. The cumulative profile of these pulses is shown at the top.

7.2. Early science observations

7.2.1. Pulsars with the LOFAR HBAs and LBAs.

We have detected many of the known, bright ($S_{400} > 50$ mJy) northern-hemisphere pulsars using both the HBAs and LBAs (Stappers et al. 2011). Some pulsars (e.g., PSRs B0329+54, B0809+74, B1508+55, and B1919+21) are even bright enough to be visible in 1 hr integrations with *individual* HBA tiles. As mentioned above, this proved quite useful for testing the beam shape, phasing, and the tracking accuracy of single, and later summed, HBA dipole elements. In the case of the LBAs, roughly a whole Dutch station (48 active dipoles) is necessary to achieve reasonable S/N within a 1 h integration on these same bright pulsars. We note that single pulses are seen with the LBAs as expected (Sect. 7.2.7).

As described earlier in Sect. 4.2.3, even individual LOFAR stations have sufficient sensitivity to be interesting for a variety of scientific applications. For example, Fig. 16 shows the average profiles resulting from the simultaneous detection of PSR B1133+16 using 96 active LBA dipoles with the Effelsberg station (called DE601) and using the 48 HBA tiles of the Dutch core station (called CS302).

The recent advent of station calibration for the LBAs discussed in Sect. 7.1.3 has led to a significant improvement in sensitivity and this is demonstrated by the observations of PSRs B0329+54, B0809+74, B0950+08, B1133+16 and B1919+21 shown in Fig. 15. These observations cover 32–80 MHz, likely making them the widest contiguous bandwidth observations ever made of radio pulsars at these frequencies. We have even been able to detect pulsars down to below 16 MHz (Stappers et al. 2011). This provides us with an unprecedented view into the evolution of the pulse profile as a function of frequency, allowing any ambiguities, for example in aligning pulse components, due to dispersive effects, to be resolved. The contributions from changing geometry, spectral index variations, scattering in the interstellar medium, and new components can be separated and

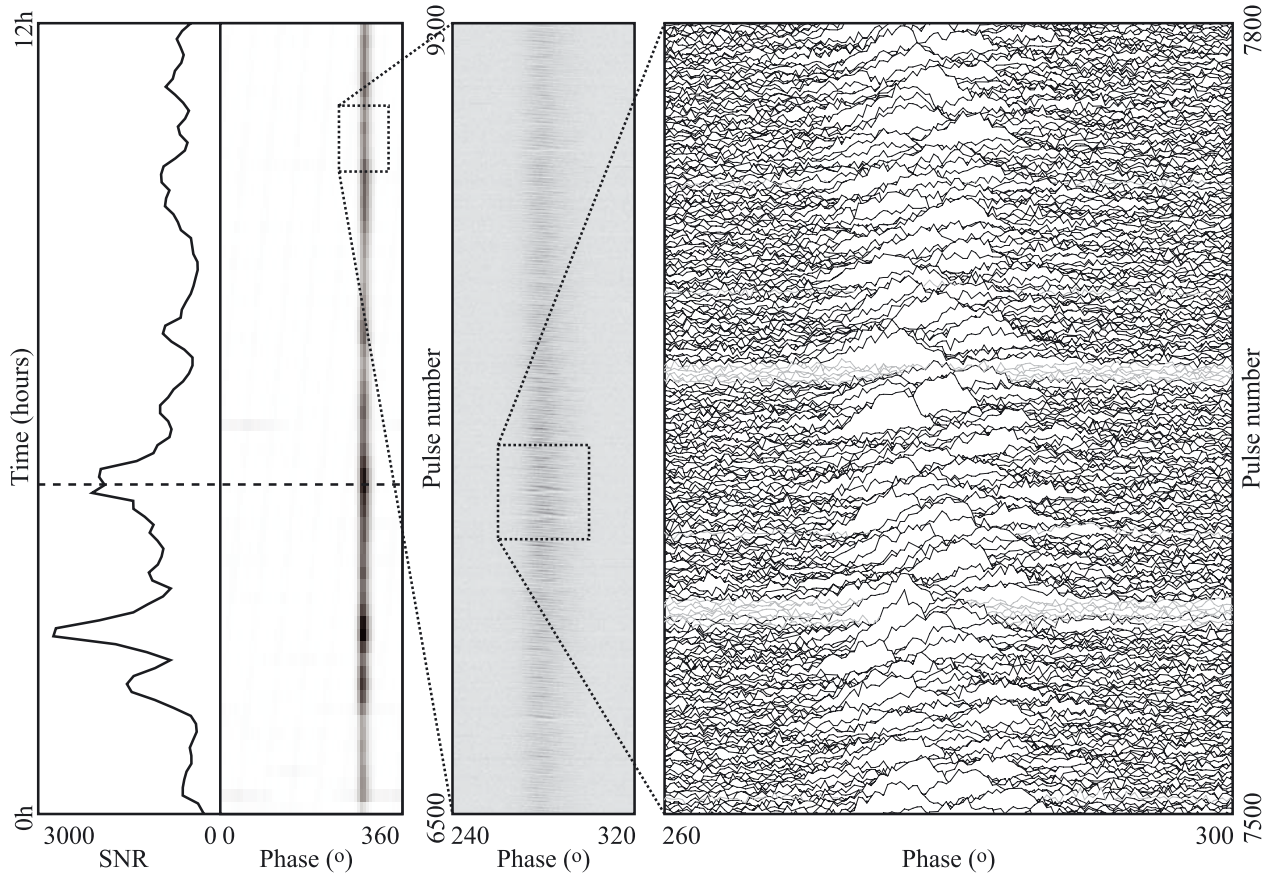

Fig. 13. A 12 h observation of PSR B0809+74 made with 4 incoherently added HBA stations in the frequency range 140–164 MHz. The *left*-most plots highlight how the S/N varies throughout the observation, mostly due to scintillation but also from the changing telescope sensitivity with zenith angle. The dashed line marks the time when the pulsar crosses the meridian. The S/N value shown in the left hand plot is calculated for each 7.2 min integration. The *middle* plot shows an hour of data when the pulsar most frequently nulled and exhibited mode changing. The *right*-most plot zooms in on two long nulls (grey), that are easily distinguished from the on-pulses (black). Note the quality of the data even in this region when the pulsar was not particularly bright, and at a high zenith angle, where the sensitivity of LOFAR is reduced by a factor of roughly two.

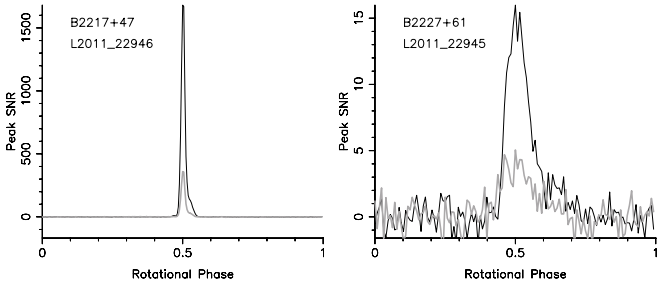

Fig. 14. The large sensitivity gain given by coherently adding the station beams is illustrated in these two sample observations. In each observation, both the incoherent *and* the coherent sum of the station beams for all 12 Superterp HBA sub-stations were recorded simultaneously. The resulting profiles were then scaled so that the off-pulse noise has a standard deviation of 1. This comparison shows the expected increase in sensitivity due to coherent summation and smaller beam size (see text for details).

studied with data like these. These data were obtained with the incoherent sum of 17 LBA stations; once we can form the coherent addition of all the stations in the LOFAR core the S/N of these observations will be improved by a further factor of about six. However we already have data of sufficient quality to start such a study. We note that dispersive effects are affecting the profiles at the lowest frequencies shown in Fig. 15; however observations with more than an order of magnitude improvement in effective time resolution are already possible. Moreover, coherent dedispersion has now been implemented which further increases the time resolution we can achieve for the least scattered pulsars.

7.2.2. Giant pulses from the Crab pulsar

The Crab pulsar, B0531+21, is particularly interesting, in part because it emits extremely bright "giant pulses" (Staelin & Reifenstein 1968; Hankins 1971). These giant pulses have the highest brightness temperature of any observed astronomical phenomenon and have been seen at frequencies from a few 10's of GHz all the way down to a few 10's of MHz (Popov et al. 2006a). LOFAR will be especially useful for studying the Crab pulsar, and other young pulsars in supernova remnants, because it will be possible to form small (arc-second to arc-minute depending on what fraction of the array is used) tied-array beams which can potentially partially resolve out these nebulae. This will greatly increase sensitivity to the pulsations over the nebular background. There are significant variations in the scattering timescale with time, as seen by Kuzmin et al. (2008), and the possibility of frequently monitoring these over a wide bandwidth with LOFAR allows one to study the changes in the nebular scattering properties on timescales ranging from the 33 ms rotation period up to years.

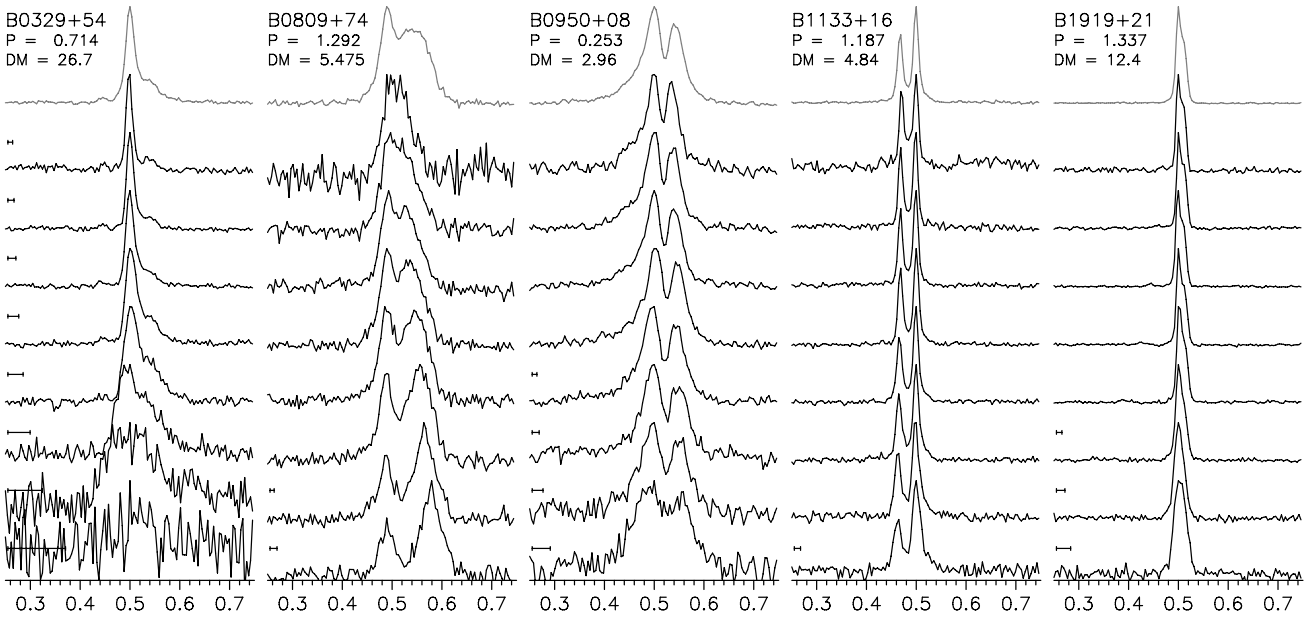

Fig. 15. A sample of average profiles of five pulsars observed with the LBAs using a total of 48 MHz with a channel bandwidth of 12.2 kHz and sampled at a rate of 1.3 ms. In all cases 17 stations were combined incoherently and the observation duration was 2 h, except for PSR B1919+21 which was observed for 1 h. The lower 8 profiles correspond to observations with 6 MHz of bandwidth centered at frequencies, from lowest to highest, of 35, 41, 47, 53, 59, 65, 71 and 77 MHz respectively. The top profile shows the summed profile from all 8 bands. At present there is no flux calibration for the LOFAR data hence no flux density scale is shown and profiles have been normalised to the peak intensity. The bar on the left hand side indicates the smearing due to dispersion across the 12.2 kHz channels and is shown only when it exceeds 3 ms. The periods are given in seconds and the dispersion measure in pc cm^{-3}.

Even before having the ability to form tied-array beams we have detected giant pulses from the Crab pulsar using the LOFAR LBAs and HBAs. Figure 8 shows a "double giant pulse", where two consecutive giant pulses are separated by only one rotation period. Note that at the observing frequency of ~150 MHz the scattering tail of each pulse is longer than the 33-ms pulse period. We have observed the Crab on a number of occassions and have already seen significant variations in this scattering timescale, indicating changes in the nebula along our line of sight. As shown in Fig. 8 we have also detected giant pulses with the LBAs in the frequency range of 32–80 MHz that exhibits a scattering tail that extends to many seconds. Studying the evolution of the scattering of these giant pulses over this sort of frequency range will be a useful probe of the frequency scaling laws appropriate for this type of scattering.

7.2.3. Multi-day observations of PSR B0809+74

Previous low-frequency monitoring of pulsars has been hampered by the limited observing times achievable by transit instruments or telescopes with equatorial mounts. In stark contrast to this, we have observed several circumpolar sources for up to 64 h continuously, using LOFAR's full tracking ability. In Fig. 13 we show a 12 h segment of one of these observations of PSR B0809+74. This corresponds to 33 000 pulses and the full data set to a remarkable 178 000 pulses. These observations used the incoherent combination of just 4 core HBA stations and yet show high S/N: the individual pulses from this pulsar are clearly visible, and the pulsar's occasional sudden turn-off, the so-called nulls, can be clearly distinguished above the low noise floor. Interspersed by nulls, the individual pulses form a drift pattern in the time versus rotational phase plane (middle and right-most panels of Fig. 13) – a well known phenomenon that provides important insight into the pulsar emission mechanism. For understanding the interaction between nulling and drifting, long integrations have been instrumental, together with the occasional, fortuitous boost in pulsar brightness through scintillation (e.g. van Leeuwen et al. 2003). Never before has a data set been gathered on a source like this with such a large number of pulses, over such a wide bandwidth and at this time resolution. These data, and more like it, will provide a unique view of the pulse emission physics continuously over timescale of milliseconds to days and we have already begun such studies.

7.2.4. Observation of the Galactic centre and PSR B1749–28

We have easily detected the bright (S_{400} = 1.1 Jy) pulsar B1749−28, which is only 1° away from the direction of the Galactic Centre (see Fig. 4 for pulse profile). Three aspects of this detection are noteworthy. First, LOFAR has adequate sensitivity to pick out a 1.1 Jy pulsed source against the high sky background in the direction of the Galactic Centre (especially considering that the single-HBA-sub-station beam is very wide at these low elevations). Second, LOFAR is able to observe bright pulsars at a zenith angle (ZA) of at least 80°. At such a high ZA, the sensitivity of the dipoles is reduced by close to a factor of 6, simply because of projection. Third, these observations were made with the incoherent sum of the stations, subsequent observations will be able to use the coherent sum of the stations reducing the size of the beam and thus resolving out part of the bright Galactic plane and further improving the sensitivity.

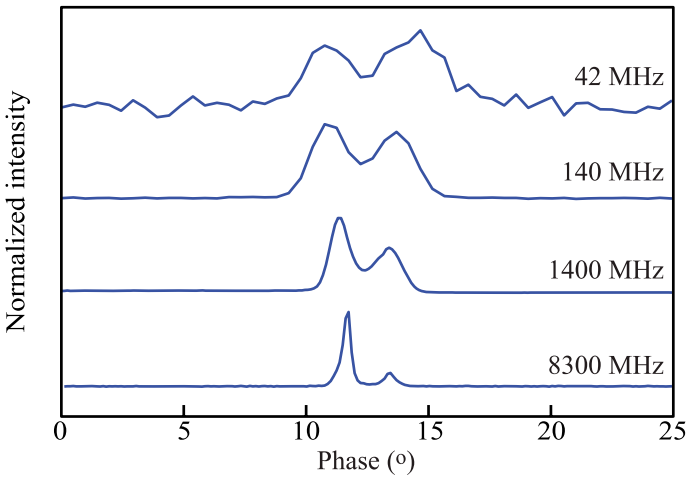

Fig. 16. PSR B1133+16's average pulse profile observed simultaneously over nearly 8 octaves in frequency. LOFAR observations were acquired in both the LBA (42 MHz, station DE601) and HBA (140 MHz, station CS302) bands and were supplemented by contemporaneous observations with the Lovell (1524 MHz) and Effelsberg (8300 MHz) telescopes.

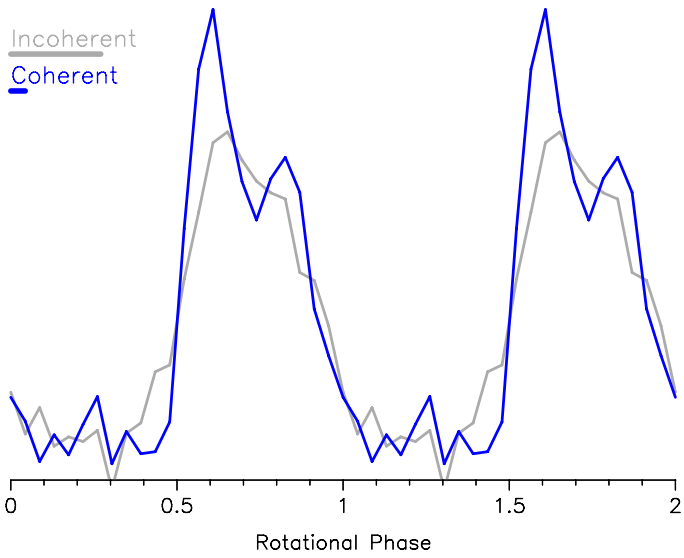

Fig. 17. For comparison, two consecutive 20-min observations of the 1.88-ms pulsar J0034-0534 at a central observing frequency of 143 MHz and with a spectral resolution of 12 kHz (corresponding time resolution of 82 μs) are shown. The data for the "Incoherent" profile has only been corrected for dispersion by applying a frequency dependent time delay to the spectral channels in the offline post-processing. In contrast, the data for the "Coherent" profile has also been coherently dedispersed online in order to remove the intra-channel dispersive smearing. The increased effective time resolution of the coherently dedispersed data is evident from comparing the two profile morphologies; e.g., two profile components are visible in the "Coherent" profile which are washed out in the "Incoherent" profile. The off-pulse noise has been scaled to the same level to facilitate comparison of the S/N. The effective time resolution is represented by the two horizontal bars on the left-hand side, and reflects the intra-channel smearing in the case of the incoherently dedispersed profile.

Furthermore, RFI may be more pernicious for observations at higher ZA. Nonetheless, this detection clearly demonstrates that it will be possible to monitor the Galactic Center for bright fast transients (though scattering will remain a major limitation).

7.2.5. Millisecond pulsars

Though scattering strongly limits the effective time resolution achievable at low observing frequencies, LOFAR is still highly capable of observing nearby MSPs, which are only mildly scattered[29]. Figure 4 shows the detections of the 16-ms pulsar J2145−0750 and the 6.2-ms pulsar B1257+12. These pulsars both have low DMs (~10 pc cm^{-3}), which made these detections possible without the need for coherent dedispersion. Despite the low DM however, one can still see that the profiles are broadened by dispersive smearing within the channels. As discussed earlier, creating narrower channels is possible but will come at the expense of the time resolution of the samples, such that the narrow pulse profile will still be poorly sampled. To circumvent this problem, we have implemented coherent dedispersion on the BG/P itself to remove intra-channel dispersive smearing and to open the possibility of observing MSPs with much larger DMs. An example of the results of observations in this mode is shown in Fig. 17. We will soon be able to do this over larger bandwidths and LOFAR will then be able to provide measurements that eclipse those achieved in Stappers et al. (2008).

7.2.6. Simultaneous LBA/HBA observations

Sub-arraying and *independent* simultaneous observations make it possible to use multiple LOFAR stations to cover a larger frequency band than the maximum 48 MHz instantaneously available from any one station. In this way, it is possible to almost[30] completely cover the 10–240 MHz radio band (see Sect. 2).

In 2009 December we performed the first LOFAR observations in which the LBA and HBA systems were used simultaneously. This was achieved by setting the Dutch core station CS302 in the HBA mode and the German station at Effelsberg (DE601) in the LBA mode and running two independent observations in parallel on the BG/P. In addition, the 76 m Lovell and 100 m Effelsberg single dish telescopes were used concurrently to record at 1.4 GHz and 8.3 GHz respectively. Figure 16 shows the cumulative pulse profile of PSR B1133+16 observed in four frequency bands centered at 42, 140, 1400, and 8300 MHz. In these initial test observations, only one station could be used for each of the LBA/HBA bands; in the future it will be possible to combine multiple stations to boost sensitivity. These data show how we can further extend the studies of the ISM and pulsar emission physics discussed in Sect. 7.2.1.

7.2.7. LBA detections of "Anomalously Intensive Pulses"

Another example of a phenomenon which may only be visible at low frequencies are the "anomalously intensive pulses" (AIPs) reported by Ulyanov et al. (2006) from five pulsars with low DMs, at decameter wavelengths with the UTR-2 radio telescope. Currently, 6 pulsars are known to emit such strong sporadic pulses at frequencies below 35 MHz (Ulyanov et al. 2006, 2007). These pulses are 10−15 ms wide with energy exceeding 10−100 times the energy of the average profile. The emission is seen to be quite narrow band with the emission typically ~1 MHz wide or seen in a few narrow 1.5–5 MHz

[29] MSPs that are further away may also have low scattering measures in some cases, as the general correlation between distance, dispersion measure, and scattering shows large deviations from the general trend, see Bhat et al. (2004).

[30] One can in principle observe in the FM band, but the data are very strongly affected by the interference from radio stations.

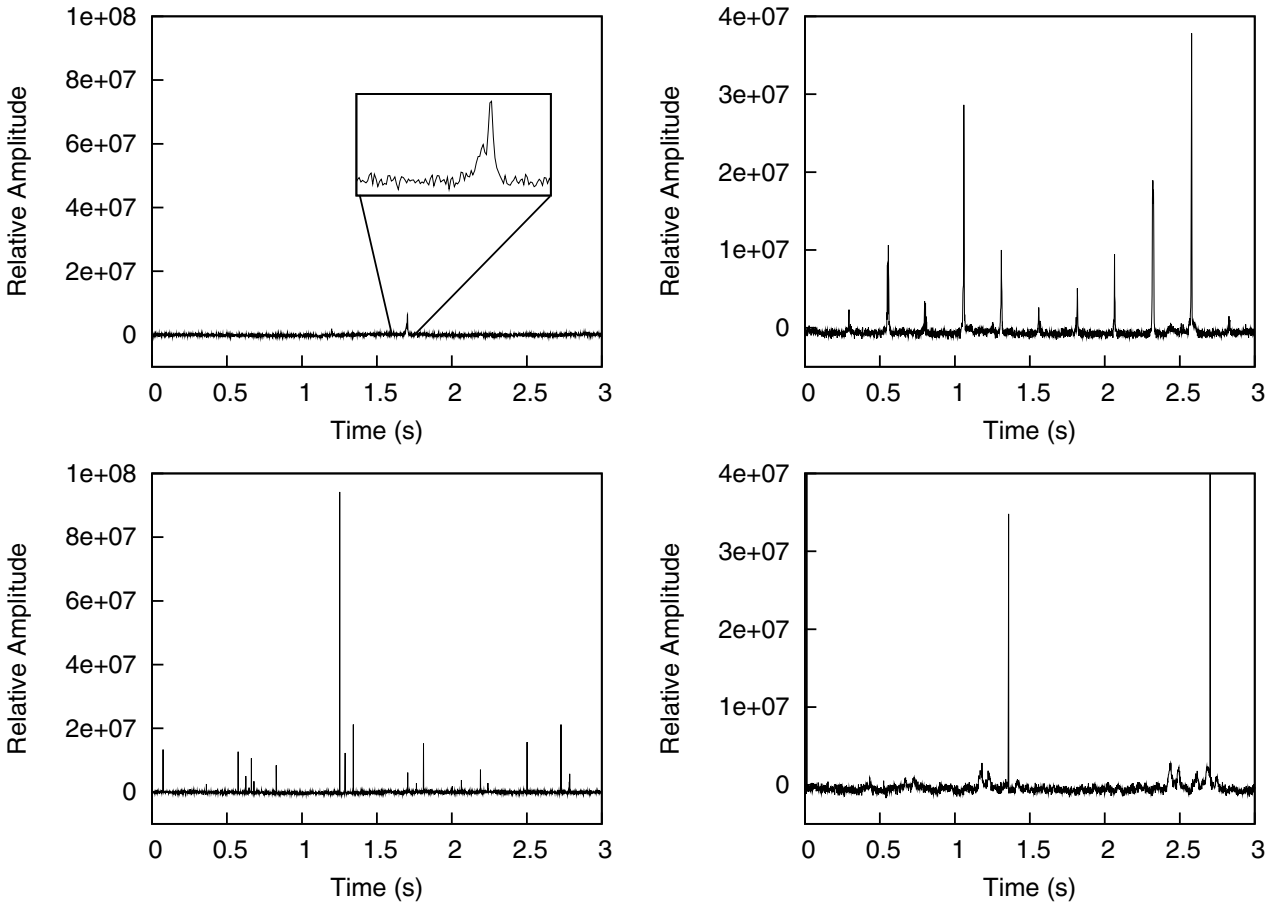

Fig. 18. Observations of PSR B0950+08 made using the LBAs (*left*) and HBAs (*right*). The *top panels* show sections of the timeseries after dedispersion to the pulsar DM of 2.96 pc cm^{-3}. We easily detect single pulses and one can see the wide range in intensity of the pulses, in particular in the low band. In the *lower panels* the same timeseries are shown but without dedipsersion, the so-called DM zero timeseries. In both the LBAs and HBAs we can see evidence for narrow spikes of RFI at zero DM, however these are clearly broadband in nature and have been completely dispersed beyond a detectable level at the dispersion measure of the pulsar. We note that the broad features seen in the DM zero timeseries of the HBAs (e.g. near 2.5 s in the lower-right panel) are due to the pulsar itself. The ordinate axes corresponds to an arbitrary amplitude but is preserved in the top and bottom plots.

frequency channels. These pulses are very intriguing but are still not carefully studied over a broad bandwidth. Such a study can shed light on a possible link between AIPs and similar phenomena observed at higher frequencies, such as giant pulses (e.g., Popov et al. 2006a; Soglasnov et al. 2004) giant micropulses (e.g. Cairns et al. 2004; Smirnova 2006), and spiky emission (Weltevrede et al. 2006). LOFAR can excel in this area, and Fig. 18 shows several examples of bright single pulses detected from PSR B0950+08.

7.2.8. Interstellar medium

As well as dispersion, several propagation effects have been proposed which could cause a frequency dependent delay in the arrival time of pulses. Many of these effects have not, as yet, been directly detected or studied. They include refractive delays, DM variations, delays associated with pulse broadening from scattering (Foster & Cordes 1990), propagation effects from within the pulsar magnetosphere (Michel 1992), and super dispersion (Shitov & Malofeev 1985; Kuzmin 1986; Shitov et al. 1988; Kuzmin et al. 2008). Many of these effects are strongly frequency dependent, with scaling indices between ν^{-3} and ν^{-5}. LOFAR is ideally suited for studying these types of effects and Fig. 19 shows a frequency-phase greyscale of simultaneous observations with the HBAs and LBAs which were dedispersed to a DM of 26.768 pc cm^{-3}. This observation corresponds to observing over more than two octaves simultaneously and so any deviation from the ν^{-2} law which is greater than ~100 ms should be visible over this large bandwidth and at these low frequencies. Once the effects have been identified we should be able to constrain how much of an impact they have on pulsar timing at higher frequencies and also extract information about the composition of the ISM.

8. Conclusions and future prospects

We have shown that LOFAR will provide a massive improvement in our ability to study pulsars and fast transients in the lowest frequency range observable from Earth (10–240 MHz). Many of these modes will also find application for observations of solar and extra-solar planets, flare stars and other time variable sources. In particular, we have discussed how wide-band, low-frequency pulsar observations will address the nature of the still enigmatic pulsar emission mechanism (Fig. 16) and will provide a useful probe of the ISM (Fig. 19). LOFAR also promises to discover many new pulsars and fast transients through the combined power of its large collecting area and (multiple) large FoVs. Through a dedicated all-sky pulsar/fast-transient survey,

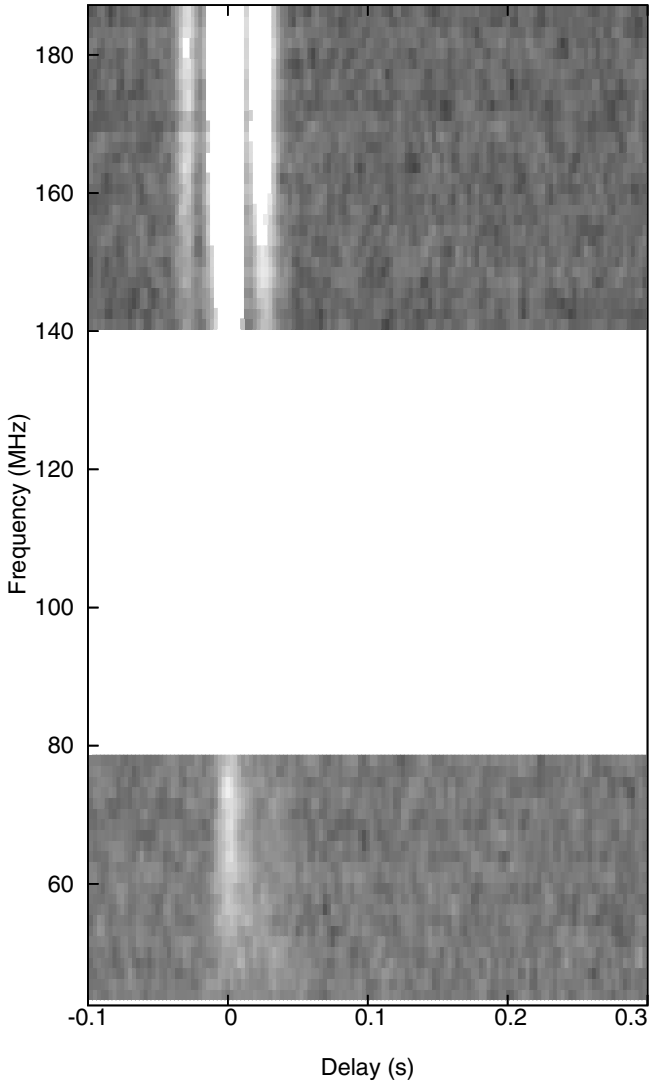

Fig. 19. An observation of PSR B0329+54 from December 2009. Data were taken using the HBAs and LBAs simultaneously. The low band data was taken using the Effelsberg international station (DE601) with 36.328125 MHz of bandwidth between 42.1875 MHz and 78.3203125 MHz. The high band data was taken using a single core station (CS302) with a bandwidth of 48.4375 MHz between 139.0625 MHz and 187.5 MHz. The figure shows no significant deviation from the ν^{-2} cold dispersion law.

a dedicated "radio-sky monitor", *and* regular piggy-backing on imaging observations, LOFAR can revolutionize our understanding of the population of rare/weak radio transients by charting parts of parameter space effectively inaccesible to traditional radio telescopes.

Though the LOFAR antennas are still in the process of being deployed in the field, the commissioning of pulsar observing modes has been underway for over 3 years, with a steady increase in the level of activity and results. Many of the desired observing modes are now functional, and have resulted in the observations presented here. While LOFAR is still in its operational infancy, it has already demonstrated several of the capabilities and technologies that make it an important precursor to the Square Kilometre Array (SKA). This includes the use of multiple digital beams to track sources widely separated on the sky (Fig. 4), simultaneous high-spatial and high-time-resolution observations (Fig. 12), and large instantaneous fractional observing bandwidth (Fig. 16).

With these successes in hand, we are focussed on continuing development of the pulsar pipelines in order to take full advantage of LOFAR's flexible data acquisition capabilities. Along with these opportunities come several challenges.

The combination of many thousands of antennas, each with "all-sky" FoV, is key to LOFAR's design. Applying proper phase corrections to add these elements and stations in phase remains one of our biggest challenges. In particular, the lack of ionospheric calibration has limited us to using stations within the Superterp, or adding stations incoherently. We are tackling this problem as part of a larger effort to provide real-time inonospheric calibration for the purposes of generating short-timescale images that can be fed into a transient detection pipeline.

Even with coherently summed, "tied-array" beams in hand, the beam pattern itself will remain very complex and requires careful study. As we have already seen from blind searches of our data, the beam response of the combined array will often allow bright pulsars to creep into observations nominally pointed far away from their position. While this might have some interesting applications, this effect is a particularly pernicious form of interference for a blind pulsar survey and requires careful treatment so that weak pulsars can still be found in the same data. This issue becomes even more delicate in the case of one-off transient events. The imaging capability of LOFAR will certainly help alleviate this problem, but care is nonetheless needed in ascribing positions to such events.

To maximize data quality and time resolution, studies of known pulsars should use coherent dedispersion. For LOFAR, this is true even for slowly rotating pulsars because the number of channels required for incoherent dedispersion quickly becomes so large as to degrade the time resolution of the data to an unacceptable level. It is already possible to apply coherent dedispersion offline to LOFAR data that is recorded as complex samples, but this mode requires a very large data rate and large amounts of offline processing. We have now also developed online coherent dedispersion (on BG/P) in order to circumvent these issues for a range of pulsars and DMs.

An all-sky pilot imaging survey with LOFAR is planned in order to address many of the outstanding calibration issues, such as beam pattern and flux density scale. This survey has as primary purpose the creation of a low-frequency sky model for future LOFAR imaging and calibration. In addition to the obvious benefits that better calibration will have for pulsar observations, this survey will also provide a platform for a commensal all-sky shallow survey using an incoherent sum of the station beams. This will be an opportunity for us to further automate and refine our data acquisition and reduction pipelines and to get the first real glimpse at what an all-sky LOFAR survey for pulsars and fast transients will offer.

Acknowledgements. LOFAR, the LOw Frequency ARray designed and constructed by ASTRON, has facilities in several countries, that are owned by various parties (each with their own funding sources), and that are collectively operated by the International LOFAR Telescope (ILT) foundation under a joint scientific policy. The data in Fig. 16 based on observations with the 100-m telescope of the MPIfR (Max-Planck-Institut für Radioastronomie) at Effelsberg and the Lovell Telescope at Jodrell Bank Observatory. Ben Stappers, Patrick Weltevrede and the Lovell observations are supported through the STFC RG R108020. Jason Hessels is a Veni Fellow of The Netherlands Organisation for Scientific Research (NWO). Joeri van Leeuwen and Thijs Coenen are supported by the Netherlands Research School for Astronomy (Grant NOVA3-NW3-2.3.1) and by the European Commission (Grant FP7-PEOPLE-2007-4-3-IRG #224838). Aris Karastergiou is grateful to the Leverhulme Trust for financial support. Ralph Wijers acknowledges support from the European

Research Council via Advanced Investigator Grant no. 247295. LVEK is supported by an ERC ST Grant.

References

Abbott, B. P., Abbott, R., Acernese, F., et al. 2010, ApJ, 713, 671
Abdo, A. A., Ackermann, M., Ajello, M., et al. 2009, Science, 325, 840
Abdo, A. A., Ackermann, M., Ajello, M., et al. 2010a, ApJS, 188, 405
Abdo, A. A., Ackermann, M., Ajello, M., et al. 2010b, ApJS, 187, 460
Abranin, E. P., Bruk, I. M., Zakharenko, V. V., & Konovalenko, A. A. 2001, Exp. Astron., 11, 85
Aharonian, F., Akhperjanian, A. G., Bazer-Bachi, A. R., et al. 2007, A&A, 466, 543
Alexov, A., Anderson, K., Bähren, L., et al. 2010a, LOFAR Data Format ICD: Beam-Formed Data, Tech. Rep., LOFAR-USG
Alexov, A., Anderson, K., Bähren, L., et al. 2010b, LOFAR Data Format ICD: File Naming Conventions, Tech. Rep., LOFAR-USG
Aliu, E., Anderhub, H., Antonelli, L. A., et al. 2008, Science, 322, 1221
Archibald, A. M., Stairs, I. H., Ransom, S. M., et al. 2009, Science, 324, 1411
Armstrong, J. W., Cordes, J. M., & Rickett, B. J. 1981, Nature, 291, 561
Armstrong, J. W., Rickett, B. J., & Spangler, S. R. 1995, ApJ, 443, 209
Asgekar, A., & Deshpande, A. A. 2005, MNRAS, 357, 1105
Beck, R. 2007, Studying Cosmic Magnetism by Polarization Observations with LOFAR
Bennett, M. F., van Eysden, C. A., & Melatos, A. 2010, MNRAS, 1370
Bhat, N. D. R., Cordes, J. M., Camilo, F., Nice, D. J., & Lorimer, D. R. 2004, ApJ, 605, 759
Boucher, C., & Altamimi, Z. 2001, http://etrs89.ensg.ign.fr/memo-V7.pdf
Bruk, I. M., & Ustimenko, B. I. 1976, Nature, 260, 766
Bruk, I. M., & Ustimenko, B. I. 1977, Ap&SS, 49, 349
Cairns, I. H., Johnston, S., & Das, P. 2004, MNRAS, 353, 270
Camilo, F., Ransom, S. M., Halpern, J. P., et al. 2006, Nature, 442, 892
Camilo, F., Ransom, S. M., Halpern, J. P., & Reynolds, J. 2007, ApJ, 666, L93
Carilli, C., & Rawlings, S. 2004, New Astron. Resv., 48, 979
Cohen, A. S., Lane, W. M., Cotton, W. D., et al. 2007, AJ, 134, 1245
Cole, T. W. 1969, Nature, 223, 487
Cordes, J. M. 1978, ApJ, 222, 1006
Cordes, J. M. 2008, in Frontiers of Astrophysics: A Celebration of NRAO's 50th Anniversary, ed. A. H. Bridle, J. J. Condon, & G. C. Hunt, ASP Conf. Ser., 395, 225
Cordes, J. M., & Lazio, T. J. W. 2002, unpublished [arXiv:astro-ph/0207156]
Cordes, J. M., & Shannon, R. M. 2010, ApJ, submitted [arXiv:1010.3785]
Cordes, J. M., Weisberg, J. M., & Hankins, T. H. 1990, AJ, 100, 1882
Cordes, J. M., Kramer, M., Lazio, T. J. W., et al. 2004a, New Astron., 48, 1413
Cordes, J. M., Lazio, T. J. W., & McLaughlin, M. A. 2004b, New Astron. Rev., 48, 1459
D'Alessandro, F. 1996, Ap&SS, 246, 73
de Vos, M., Gunst, A. W., & Nijboer, R. 2009, IEEE Proc., 97, 1431
Deshpande, A. A., & Radhakrishnan, V. 1994, J. Astrophys. Astron., 15, 329
Deshpande, A. A., Shevgaonkar, R. K., & Shastry, C. V. 1989, J. Inst. Electron. Telecommunications Eng.
Edwards, R. T., & Stappers, B. W. 2003, A&A, 407, 273
Ellingson, S. W., Clarke, T. E., Cohen, A., et al. 2009, IEEE Proc., 97, 1421
Falcke, H., & LOFAR Cosmic Ray Key Science Project. 2007, Astron. Nachr., 328, 593
Faucher-Giguère, C.-A., & Kaspi, V. M. 2006, ApJ, 643, 332
Fender, R. P., Wijers, R. A. M. J., Stappers, B., et al. 2006, in VI Microquasar Workshop: Microquasars and Beyond
Fender, R., Wijers, R., Stappers, B., & LOFAR Transients Key Science Project 2008 [arXiv:0805.4349]
Foster, R. S., & Cordes, J. M. 1990, ApJ, 364, 123
Fruchter, A. S., Stinebring, D. R., & Taylor, J. H. 1988, Nature, 333, 237
Golap, K., Shankar, N. U., Sachdev, S., Dodson, R., & Sastry, C. V. 1998, J. Astrophys. Astron., 19, 35
Gould, D. M., & Lyne, A. G. 1998, MNRAS, 301, 235
Gupta, Y., Gothoskar, P., Joshi, B. C., et al. 2000, in Pulsar Astronomy – 2000 and Beyond, ed. M. Kramer, N. Wex, & R. Wielebinski, ASP Conf. Ser., 202, IAU Colloq., 177, 277
Gurevich, A., Beskin, V., & Istomin, Y. 1993, Physics of the Pulsar Magnetosphere, ed. A. Gurevich, V. Beskin, & Y. Istomin (Cambridge, UK: Cambridge University Press), 432
Hamaker, J. P., Bregman, J. D., & Sault, R. J. 1996, A&AS, 117, 137
Han, J. 2009, in IAU Symp., 259, 455
Hankins, T. H. 1971, ApJ, 169, 487
Heald, G., McKean, J., Pizzo, R., et al. 2010 [arXiv:1008.4693]
Hessels, J., Stappers, B., Alexov, A., et al. 2010 [arXiv:1009.1758]
Hessels, J. W. T., Stappers, B. W., van Leeuwen, J., & The LOFAR Transients Key Science Project 2009, in ASP Conf. Ser., ed. D. J. Saikia, D. A. Green, Y. Gupta, & T. Venturi, 407, 318
Hessels, J. W. T., Roberts, M. S. E., & McLaughlin, M. 2011, in Radio Pulsars: a key to unlock the secrets of the Universe, ed. A. Possenti, AIP Proc., 999
Hewish, A., Bell, S. J., Pilkington, J. D. H., Scott, P. F., & Collins, R. A. 1968, Nature, 217, 709
Intema, H. T. 2009, Ph.D. Thesis, Leiden Observatory, Leiden University, PO Box 9513, 2300 RA Leiden, The Netherlands
Izvekova, V. A., Jessner, A., Kuzmin, A. D., et al. 1994, A&AS, 105, 235
Jenet, F. A., Anderson, S. B., & Prince, T. A. 2001, ApJ, 546, 394
Johnston, H. M., & Kulkarni, S. R. 1991, ApJ, 368, 504
Karastergiou, A., von Hoensbroech, A., Kramer, M., et al. 2001, A&A, 379, 270
Karastergiou, A., Johnston, S., & Kramer, M. 2003, A&A, 404, 325
Karuppusamy, R., Stappers, B., & van Straten, W. 2008, PASP, 120, 191
Karuppusamy, R., Stappers, B. W., & Serylak, M. 2011, A&A, 525, A55
Keane, E. F., & Kramer, M. 2008, MNRAS, 391, 2009
Keith, M. J., Jameson, A., van Straten, W., et al. 2010, MNRAS, 1356
Kondratiev, V. I., McLaughlin, M. A., Lorimer, D. R., et al. 2009, ApJ, 702, 692
Kramer, M., Wielebinski, R., Jessner, A., Gil, J. A., & Seiradakis, J. H. 1994, A&AS, 107, 515
Kramer, M., Xilouris, K. M., Lorimer, D. R., et al. 1998, ApJ, 501, 270
Kramer, M., Lange, C., Lorimer, D. R., et al. 1999, ApJ, 526, 957
Kramer, M., Karastergiou, A., Gupta, Y., et al. 2003, A&A, 407, 655
Kramer, M., Lyne, A. G., O'Brien, J. T., Jordan, C. A., & Lorimer, D. R. 2006, Science, 312, 549
Kuzmin, A., Losovsky, B. Y., Jordan, C. A., & Smith, F. G. 2008, A&A, 483, 13
Kuzmin, A. D., & Losovskii, B. Y. 1997, Astron. Lett., 23, 283
Kuzmin, A. D., & Losovsky, B. Y. 2001, A&A, 368, 230
Kuzmin, A. D., Malofeev, V. M., Shitov, Y. P., et al. 1978, MNRAS, 185, 441
Lawson, K. D., Mayer, C. J., Osborne, J. L., & Parkinson, M. L. 1987, MNRAS, 225, 307
Levin, L., Bailes, M., Bates, S., et al. 2010, ApJ, 721, L33
Löhmer, O., Mitra, D., Gupta, Y., Kramer, M., & Ahuja, A. 2004, A&A, 425, 569
Lonsdale, C. J., Cappallo, R. J., Morales, M. F., et al. 2009, IEEE Proc., 97, 1497
Lorimer, D. R., & Kramer, M. 2005, Handbook of Pulsar Astronomy (Cambridge University Press)
Lorimer, D. R., Faulkner, A. J., Lyne, A. G., et al. 2006, MNRAS, 372, 777
Lorimer, D. R., Bailes, M., McLaughlin, M. A., Narkevic, D. J., & Crawford, F. 2007, Science, 318, 777
Lyne, A. G., & Smith, F. G. 2004, Pulsar Astronomy, 3rd ed. (Cambridge: Cambridge University Press), 777
Lyne, A., Hobbs, G., Kramer, M., Stairs, I., & Stappers, B. 2010, Science, 329, 408
Lyutikov, M. 2002, ApJ, 580, L65
Malofeev, V. M. 2000, in Pulsar Astronomy – 2000 and Beyond, ed. M. Kramer, N. Wex, & R. Wielebinski, IAU Colloq., 177, ASP Conf. Ser., 202, 221
Malofeev, V. M., & Malov, O. I. 1997, Nature, 389, 697
Malofeev, V. M., Gil, J. A., Jessner, A., et al. 1994, A&A, 285, 201
Malofeev, V. M., Malov, O. I., & Shchegoleva, N. V. 2000, Astron. Rep., 44, 436
Malofeev, V. M., Malov, O. I., Teplykh, D. A., Tyul'Bashev, S. A., & Tyul'Basheva, G. E. 2005, Astron. Rep., 49, 242
Malofeev, V. M., Malov, O. I., & Teplykh, D. A. 2006, Chin. J. Astron. Astrophys. Suppl. 2, 6, 68
Malofeev, V. M., Malov, O. I., & Teplykh, D. A. 2007, Ap&SS, 308, 211
Malov, O. I., & Malofeev, V. M. 2010, Astron. Rep., 54, 210
Manchester, R. N., Hobbs, G. B., Teoh, A., & Hobbs, M. 2005, AJ, 129, 1993
Maron, O., Kijak, J., Kramer, M., & Wielebinski, R. 2000, A&AS, 147, 195
McLaughlin, M. A., & Cordes, J. M. 2003, ApJ, 596, 982
McLaughlin, M. A., Lyne, A. G., Lorimer, D. R., et al. 2006, Nature, 439, 817
McLaughlin, M. A., Lyne, A. G., Keane, E. F., et al. 2009, MNRAS, 400, 1431
Melrose, D. 2004, in Young Neutron Stars and Their Environments, ed. F. Camilo, & B. M. Gaensler (San Francisco: ASP), IAU Symp., 218, 349
Mitra, D., & Rankin, J. M. 2002, ApJ, 577, 322
Mol, J. D., & Romein, J. W. 2011, The LOFAR Beam Former: Implementation and Performance Analysis, under review
Morris, D., Kramer, M., Thum, C., et al. 1997, A&A, 322, L17
Narayan, R. 1992, Philos. Trans. Roy. Soc. London A, 341, 151
Navarro, J., de Bruyn, G., Frail, D., Kulkarni, S. R., & Lyne, A. G. 1995, ApJ, 455, L55
Nijboer, R. J., & Noordam, J. E. 2007, in Astronomical Data Analysis Software and Systems XVI, ed. R. A. Shaw, F. Hill, & D. J. Bell, ASP Conf. Ser., 376, 237
Noutsos, A., Johnston, S., Kramer, M., & Karastergiou, A. 2008, MNRAS, 386, 1881

Petrova, S. A. 2006, MNRAS, 368, 1764
Petrova, S. A. 2008, MNRAS, 383, 1413
Popov, M. V., Kuzmin, A. D., Ulyanov, O. M., et al. 2006a, On the Present and Future of Pulsar Astronomy, 26th meeting of the IAU, Joint Discussion 2, 16–17 August, Prague, Czech Republic, JD02, #19, 2
Popov, M. V., Kuzmin, A. D., Ul'yanov, O. M., et al. 2006b, Astron. Rep., 50, 562
Rankin, J. M. 1993, ApJ, 405, 285
Rankin, J. M., Comella, J. M., Craft, H. D., et al. 1970, ApJ, 162, 707
Ransom, S. M., Cordes, J. M., & Eikenberry, S. S. 2003, ApJ, 589, 911
Ransom, S. M., Ray, P. S., Camilo, F., et al. 2011, ApJ, 727, L16
Reich, P., & Reich, W. 1988, A&AS, 74, 7
Rickett, B. J. 1970, MNRAS, 150, 67
Rickett, B. J. 1990, ARA&A, 28, 561
Rickett, B., Johnston, S., Tomlinson, T., & Reynolds, J. 2009, MNRAS, 395, 1391
Roger, R. S., Costain, C. H., Landecker, T. L., & Swerdlyk, C. M. 1999, A&AS, 137, 7
Romein, J. W., Broekema, P. C., Mol, J. D., & van Nieuwpoort, R. V. 2010, in ACM Symposium on Principles and Practice of Parallel Programming (PPoPP'10), Bangalore, India, 169
Ryabov, V. B., Vavriv, D. M., Zarka, P., et al. 2010, A&A, 510, A16
Shishov, V. I., & Smirnova, T. V. 2002, Astron. Rep., 46, 731
Shitov, Y. P., & Pugachev, V. D. 1997, New Astr., 3, 101
Shitov, Y. P., Malofeev, V. M., & Izvekova, V. A. 1988, SvA Lett., 14, 181
Shrauner, J. A., Taylor, J. H., & Woan, G. 1998, ApJ, 509, 785
Singh, K., Bähren, L., Falcke, H., et al. 2008, in International Cosmic Ray Conference, 4, 429
Slee, O. B., Alurkar, S. K., & Bobra, A. D. 1986, Aust. J. Phys., 39, 103
Smirnova, T. V. 2006, Astron. Rep., 50, 915
Smirnova, T. V., & Shishov, V. I. 2010, Astron. Rep., 54, 139
Smirnova, T. V., Tul'bashev, S. A., & Boriakoff, V. 1994, A&A, 286, 807
Soglasnov, V. A., Popov, M. V., & Kuzmin, O. A. 1983, AZh, 60, 293
Soglasnov, V. A., Popov, M. V., Bartel, N., et al. 2004, ApJ, 616, 439
Staelin, D. H., & Reifenstein, III, E. C. 1968, Science, 162, 1481
Stappers, B. W., Bailes, M., Lyne, A. G., et al. 1996, ApJ, 465, L119
Stappers, B. W., van Leeuwen, A. G. J., Kramer, M., Stinebring, D., & Hessels, J. 2007, in WE-Heraeus Seminar on Neutron Stars and Pulsars 40 years after the Discovery, ed. W. Becker, & H. H. Huang, 100
Stappers, B. W., Karappusamy, R., & Hessels, J. W. T. 2008, in 40 Years of Pulsars: Millisecond Pulsars, Magnetars and More, ed. C. Bassa, Z. Wang, A. Cumming, & V. M. Kaspi, AIP Conf. Ser., 983, 593
Stappers, B. W., Hessels, J., Alexov, A., et al. 2011, in Radio Pulsars: a key to unlock the secrets of the Universe, AIP Conf. Ser., 1357
Stinebring, D. R., McLaughlin, M. A., Cordes, J. M., et al. 2001, ApJ, 549, L97
Swarup, G., Ananthakrishnan, S., Kapahi, V. K., et al. 1991, Current Science, 60, 95
Tang, A. P. S., & Cheng, K. S. 2001, ApJ, 549, 1039
Tavani, M., Barbiellini, G., Argan, A., et al. 2009, A&A, 502, 995
Team, I. B. G. 2008, IBM J. Res. Dev., 52
Thompson, D. J. 2000, Adv. Space Res., 25, 659
Tinbergen, J. 1996, Astronomical Polarimetry (Cambridge University Press), iSBN: 0521475317
Ulyanov, O. M., Zakharenko, V. V., Konovalenko, A. A., et al. 2006, Radiofizika and Radioastronomia, 11, 113
Ulyanov, O. M., Deshpande, A. A., Zakharenko, V. V., Asgekar, A., & Shankar, U. 2007, Radiofizika and Radioastronomia, 12, 5
Ul'Yanov, O. M., Zakharenko, V. V., & Bruk, I. M. 2008, Astron. Rep., 52, 917
van der Horst, A. J., Kamble, A., Resmi, L., et al. 2008, A&A, 480, 35
van Eysden, C. A., & Melatos, A. 2010, MNRAS, 1459
van Leeuwen, J., & Stappers, B. W. 2010, A&A, 509, A7
van Leeuwen, A. G. J., Stappers, B. W., Ramachandran, R., & Rankin, J. M. 2003, A&A, 399, 223
Van Riper, K. A., Epstein, R. I., & Miller, G. S. 1991, ApJ, 381, L17
van Straten, W. 2004, ApJS, 152, 129
van Straten, W., Manchester, R. N., Johnston, S., & Reynolds, J. E. 2010, PASA, 27, 104
von Hoensbroech, A., & Xilouris, K. M. 1997, A&AS, 126, 121
Vranesevic, N., Manchester, R. N., Lorimer, D. R., et al. 2004, ApJ, 617, L139
Welch, J., Backer, D., Blitz, L., et al. 2009, IEEE Proc., 97, 1438
Weltevrede, P., Stappers, B. W., van den Horn, L. J., & Edwards, R. T. 2003, A&A, 412, 473
Weltevrede, P., Wright, G. A. E., Stappers, B. W., & Rankin, J. M. 2006, A&A, 458, 269
Weltevrede, P., Stappers, B. W., & Edwards, R. T. 2007, A&A, 469, 607
Wijnholds, S. J., & van der Veen, A. 2009, IEEE Transactions on Signal Processing, 57, 3512
Wijnholds, S. J., & van der Veen, A. 2010b, in Proc. 17th European Signal Processing Conference (EuSiPCo) [arXiv:1003.2497v1]
Wijnholds, S., van der Tol, S., Nijboer, R., & van der Veen, A. 2010a, IEEE Signal Processing Magazine, 27, 30
Wolleben, M., Fletcher, A., Landecker, T. L., et al. 2010, ApJ, 724, L48
You, X. P., Hobbs, G., Coles, W. A., et al. 2007, MNRAS, 378, 493

[1] Jodrell Bank Center for Astrophysics, School of Physics and Astronomy, The University of Manchester, M13 9PL Manchester, UK
e-mail: Ben.Stappers@manchester.ac.uk
[2] Netherlands Institute for Radio Astronomy (ASTRON), Postbus 2, 7990 AA Dwingeloo, The Netherlands
[3] Astronomical Institute "Anton Pannekoek", University of Amsterdam, Postbus 94249, 1090 GE Amsterdam, The Netherlands
[4] Astrophysics, University of Oxford, Denys Wilkinson Building, Keble Road, Oxford OX1 3RH, UK
[5] Max-Planck-Institut für Radioastronomie, Auf dem Hügel 69, 53121 Bonn, Germany
[6] School of Physics and Astronomy, University of Southampton, Southampton, SO17 1BJ, UK
[7] Max Planck Institute for Astrophysics, Karl Schwarzschild Str. 1, 85741 Garching, Germany
[8] Department of Physics & Astronomy, Hicks Building, Hounsfield Road, Sheffield S3 7RH, UK
[9] Leiden Observatory, Leiden University, PO Box 9513, 2300 RA Leiden, The Netherlands
[10] Kapteyn Astronomical Institute, PO Box 800, 9700 AV Groningen, The Netherlands
[11] Onsala Space Observatory, Dept. of Earth and Space Sciences, Chalmers University of Technology, SE-43992 Onsala, Sweden
[12] Department of Astrophysics/IMAPP, Radboud University Nijmegen, PO Box 9010, 6500 GL Nijmegen, The Netherlands
[13] International Centre for Radio Astronomy Research – Curtin University, GPO Box U1987, Perth, WA 6845, Australia
[14] STFC Rutherford Appleton Laboratory, Harwell Science and Innovation Campus, Didcot OX11 0QX, UK
[15] Institute for Astronomy, University of Edinburgh, Royal Observatory of Edinburgh, Blackford Hill, Edinburgh EH9 3HJ, UK
[16] LESIA, UMR CNRS 8109, Observatoire de Paris, 92195 Meudon, France
[17] Argelander-Institut für Astronomie, University of Bonn, Auf dem Hügel 71, 53121 Bonn, Germany
[18] Leibniz-Institut fr Astrophysik Potsdam (AIP), An der Sternwarte 16, 14482 Potsdam, Germany
[19] Thüringer Landessternwarte, Sternwarte 5, 07778 Tautenburg, Germany
[20] Astronomisches Institut der Ruhr-Universität Bochum, Universitaetsstrasse 150, 44780 Bochum, Germany
[21] Jacobs University Bremen, Campus Ring 1, 28759 Bremen, Germany
[22] Laboratoire de Physique et Chimie de l'Environnement et de l'Espace, CNRS/Université d'Orléans, France
[23] Center for Information Technology (CIT), University of Groningen, The Netherlands
[24] Radio Astronomy Lab, UC Berkeley, CA, USA
[25] Centre de Recherche Astrophysique de Lyon, Observatoire de Lyon, 9 Av. Charles André, 69561 Saint Genis Laval Cedex, France
[26] Mt Stromlo Observatory, Research School of Astronomy and Astrophysics, Australian National University, Weston, A.C.T. 2611, Australia